

Parallel Implementation of Concentrated Solar Power and Energy Storage into the Brayton Cycle

by

Blake R. Lopez

A THESIS

submitted to

Oregon State University

Honors College

in partial fulfillment of

the requirements for the

degree of

Honors Baccalaureate of Science in Chemical Engineering

(Honors Scholar)

Presented May 27, 2020

Commencement June 2020

AN ABSTRACT OF THE THESIS OF

Blake Lopez for the degree of Honors Baccalaureate of Science in Chemical Engineering presented on May 27, 2020.

Title: Parallel Implementation of Concentrated Solar Power and Energy Storage into the Brayton Cycle.

Abstract approved: _____

Nicholas AuYeung

Concentrated solar power (CSP) along with thermal energy storage (TES) has the potential to provide reliable energy from an intermittent source. TES is used to store energy while the sun is shining, allowing for the stored energy to be used when the sun is no longer shining. There are many types of TES that can be used but thermochemical energy storage (TCES) has unique capabilities that makes it more desirable than other technologies. TCES can be stored indefinitely using a reversible reaction with high energy density.

Air can be used to directly transfer heat to and from a BaO/BaO₂ cycle, a type of TCES, during both on and off sun hours. This ability means the BaO/BaO₂ cycle can be integrated with a compressor, gas turbine, and CSP to produce consistent energy from an intermittent source. This eliminates the number heat exchangers and working fluid involved in the power plant.

This combination was modeled using MATLAB in a parallel configuration with limited complexity to determine the efficiency and viability of this TCES technology for a 50 MW_e plant with 16 hours of off sun storage for continuous power production. Cycle solar to electric conversions of 6-12% were achieved for this system at a maximum receiver temperature of 1600 K. The efficiency of this simple system warrants further analysis into the economics of the system to determine whether or not the system is truly viable.

Key Words: Solar Thermal Energy, Thermochemical Energy Storage, Concentrated Solar Power

Corresponding email address: lopezbl@oregonstate.edu

©Copyright by Blake R. Lopez

May 27, 2020

Parallel Implementation of Concentrated Solar Power and Energy Storage into the Brayton Cycle

by

Blake R. Lopez

A THESIS

submitted to

Oregon State University

Honors College

in partial fulfillment of

the requirements for the

degree of

Honors Baccalaureate of Science in Chemical Engineering

(Honors Scholar)

Presented May 27, 2020

Commencement June 2020

Honors Baccalaureate of Science in Chemical Engineering project of Blake R. Lopez presented on May 27, 2020.

APPROVED:

Nicholas AuYeung, Mentor, representing Chemical Engineering

Chih-Hung Chang, Committee Member, representing Chemical Engineering

Brian Wood, Committee Member, representing Environmental Engineering

Toni Doolen, Dean, Oregon State University Honors College

I understand that my project will become part of the permanent collection of Oregon State University, Honors College. My signature below authorizes release of my project to any reader upon request.

Blake R. Lopez, Author

TABLE OF CONTENTS

Background	1
Solar Thermal Energy	1
Thermal Energy Storage	2
Sensible Heat	2
Latent Heat	2
Thermochemical Energy Storage	3
Brayton Cycle	3
General Brayton Cycle	3
Combustion	5
Computational Approach	6
Reason for Approach	6
Parallel vs Serial	6
Metal Oxide TCES	7
CSP and TCES in a Brayton Cycle	8
Barium Oxide-Peroxide Energy Storage	10
Approach	11
Key Equations	14
Brayton Cycle	14
Rankine Cycle	15
Cycle	15
Results and Discussion	16
Charging	16
Discharging	17
Complete Cycle	20
HYSYS Validation	25
Conclusion	27
Future Work	27
References	28
Appendix	30
Key MATLAB Codes	30
Functions	30
Complete Cycle	37

Background

Solar Thermal Energy

The total primary energy of the world could be entirely met by solar energy several times over but faces issues of intermittency and availability [1], [2]. Concentrated solar power (CSP) combined with thermal energy storage (TES) is a region specific way of addressing the issue of intermittency [3]. By storing some of the energy from the sun during the day using a TES technology, a CSP facility can still produce energy during the night and during cloudy times. TES can be implemented in three different ways: sensible, latent, and thermochemical energy storage (TCES). Sensible heat stores energy by increasing the temperature of the storage material. Latent heat stores energy the phase change of a material (melting or evaporating). TCES stores energy using a reversible chemical reaction.

There are positives and negatives associated with each of these technologies but one the most important metrics of TES technologies is the energy density which is illustrated in Figure 1. It can be observed the energy of TCES is approximately 5 to 10 times greater than the other technologies [3]. The large energy density of TCES can result in lower energy costs.

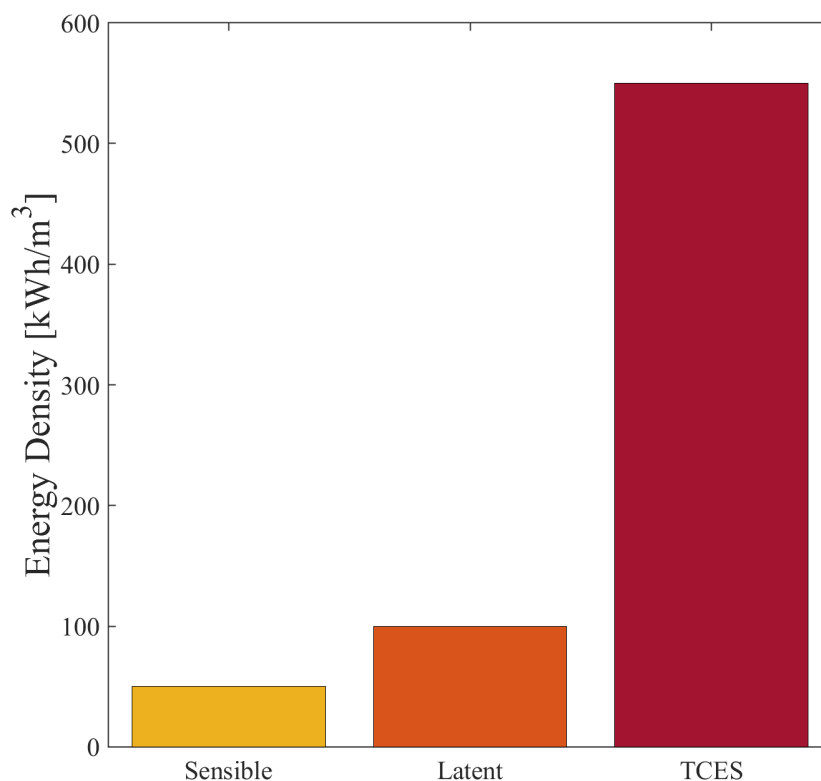


Figure 1 - Energy density of the three different TES technologies adapted from Alava et al. [3]

Thermal Energy Storage

Sensible Heat

Sensible heat storage occurs with the increased temperature of a material without a phase change. The key metric for sensible heat storage is the specific heat capacity of the material; the higher the specific heat capacity, the more energy can be stored. The total energy stored can be determined from Equation 1.

$$Q = \int_{T_1}^{T_2} m \hat{C}_p dT$$

$$Q = \text{energy stored [=} [J]$$

$$T = \text{temperature [=} [K]$$

$$m = \text{mass of storage material [=} [kg]$$

$$\hat{C}_p = \text{mass specific heat capacity [=} [\frac{J}{kgK}]$$
(1)

Materials with a high specific heat such as molten salts, thermal oils, and liquid metals are chosen depending on the desired temperature range [4]. In practice, molten salts have been used at temperatures exceeding 400 °C but less than 600 °C in CSP facilities by circulating the molten salt from a cold storage tank through the receiver to a hot storage tank [4]. There have also been studies into the use of liquid metals as storage materials due to their high operating temperatures but face issues of low energy density. Overall sensible heat storage has been the most studied form of TES, but the lower energy density and lower operating temperatures limit the efficiency of the power cycle that goes along with them [5].

Latent Heat

Latent heat stores energy in the phase change of a material so they are often called phase change materials (PCM). The key metric for PCM is the heat of fusion whether it is solid to liquid, liquid to gas, solid to solid, or others. The energy stored in a PCM can be determined by Equation 2.

$$Q = m \Delta \hat{h}_{fus}$$

$$Q = \text{energy stored [=} [J]$$

$$m = \text{mass of storage material [=} [kg]$$

$$\Delta \hat{h}_{fus} = \text{heat of fusion [=} [\frac{J}{kg}]$$
(2)

While evaporation has a high specific enthalpy difference associated with it, the low density of a vapor makes it difficult to store the energy economically. The most simple form of a PCM for a CSP plant is storing excess steam generated for use in a Rankine Cycle [3], [6]. As a result solid to liquid transitions with a high heat of fusion such as paraffins (at low temperatures), salts, and

salt eutectics (higher temperatures) are often chosen [3], [7]. Additionally, PCMs face issues of low thermal conductivity that impact their performance.

Thermochemical Energy Storage

Thermochemical energy storage (TCES) has the highest energy density when compared to sensible and latent heat energy storage. This high energy density is accomplished by using a reversible chemical reaction to store and release energy. When the sun is shining, the heat input from the sun drives the endothermic reaction forward. Then, when the sun is no longer shining, the reverse exothermic reaction can be run to release the stored energy. While sensible and latent heat storage is limited to the quality of insulation, TCES can be stored indefinitely when the products of the endothermic reaction are separated [8]. The energy that can be stored for a TCES system can be determined by Equation 3.

$$\begin{aligned}
 Q &= m \Delta \hat{h}_{react} \\
 Q &= \text{energy stored [=} [J] \\
 m &= \text{mass of storage material [=} [kg] \\
 \Delta \hat{h}_{react} &= \text{heat of reaction [=} [\frac{J}{kg}]
 \end{aligned}
 \tag{3}$$

Examples of TCES include dehydration of a salt, the redox reaction of metal oxides and carbonation reactions, and many more [3]. Additionally, calcium looping with a CO₂ power cycle has been of interest because of the high efficiency associated with the power cycle [8]. A key benefit of these reactions is they can operate at higher temperatures than most sensible and latent materials. This ability allows for the use of higher efficiency power cycles [9].

Brayton Cycle

General Brayton Cycle

A Brayton Cycle consists of four main components: compressor, heater, gas turbine, and cooler, as seen in Figure 2. Air is the most common working fluid for Brayton Cycles but the use of other working fluids such as supercritical CO₂ allows for higher efficiencies [10]. The key design parameter is the compression ratio. Increasing the compression ratio increases the efficiency of the Brayton Cycle but is limited by materials of construction as increasing the compression ratio increases the operating temperatures throughout the process. Figure 3 illustrates the impact of the compression ratio on the thermal efficiency of the cycle. Two other important factors are the isentropic efficiencies of the compressor and turbine. Higher isentropic efficiencies are desirable because it means there are less energy losses due to 2nd Law constraints.

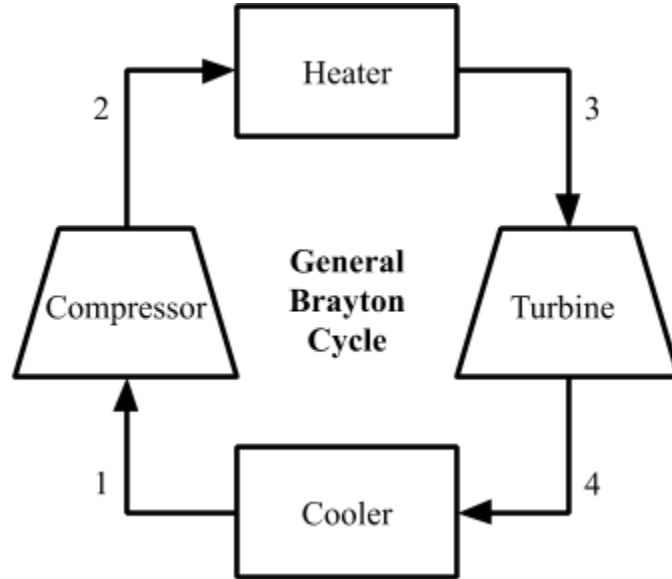


Figure 2 - General closed Brayton Cycle

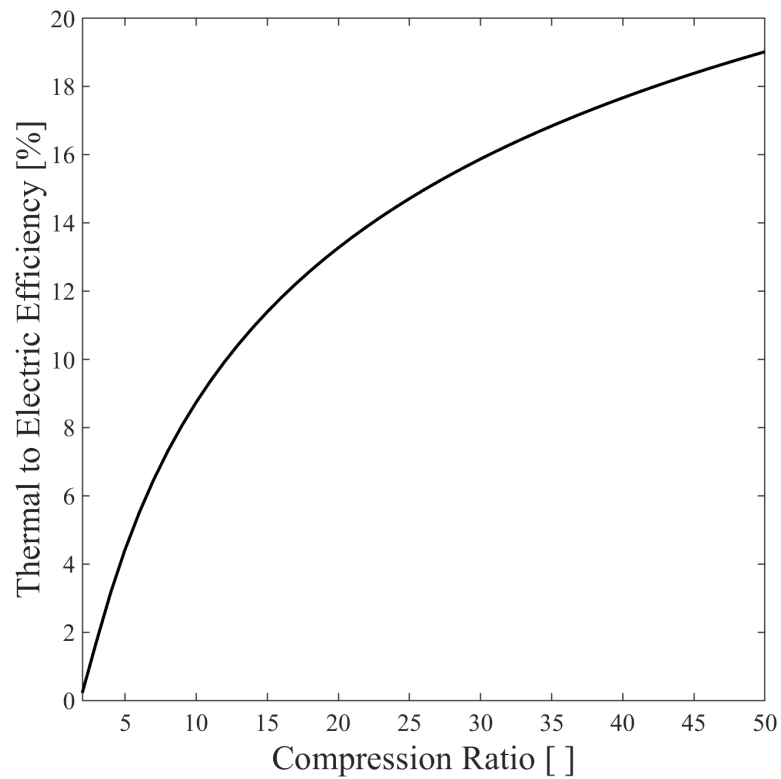


Figure 3 - Example efficiency of the Brayton Cycle with a temperature difference of 500 K across the heater, compressor inlet temperature of 298 K and pressure of 1 bar.

Combustion

By using a combustion chamber in place of a heater, the turbine outlet does not recycle back to the compressor but allows for fuels like natural gas to be used to generate electricity as illustrated in Figure 4. With the addition of a fuel source, an additional design parameter is introduced as different fuels can be used depending upon availability and operating pressures. A key benefit of combustion is flow rates can be easily adjusted to fit power demands which is why Natural Gas power plants are often used in conjunction with renewable energy sources to levelize the fluctuations in energy supplied from renewables.

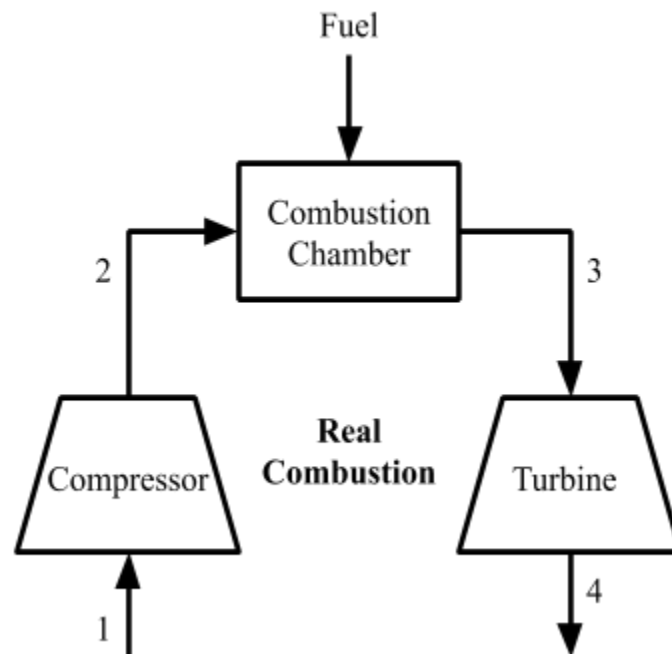


Figure 4 -Brayton cycle combustion

Computational Approach

Reason for Approach

Parallel vs Serial

Electricity production with CSP and TCES has two main configurations while charging (i.e when the sun is shining): parallel and serial. In a parallel configuration, as seen in Figure 5, the high energy output from the solar field is split and some of the energy goes towards storing energy and the rest goes towards generating electricity. While in a serial configuration, as seen in Figure 6, the high energy output from the solar field is first used to store energy before the rest of the energy is used to generate electricity.

Depending upon the gas-solid contacting pattern of the TCES, one configuration is more advantageous than the other. For a fluidized bed or falling particle reactor, a serial configuration is more appropriate because the relatively small pressure drop and uniform temperature associated with it means the exit stream is at conditions favorable for a power block [11]. A packed bed reactor with a high pressure drop would significantly decrease the performance of the power block in a serial configuration so a parallel configuration is more efficient [11]. Additionally, with lower outlet temperature of the packed bed, it is more beneficial to have outlet as close to ambient conditions to maximize the energy storage.

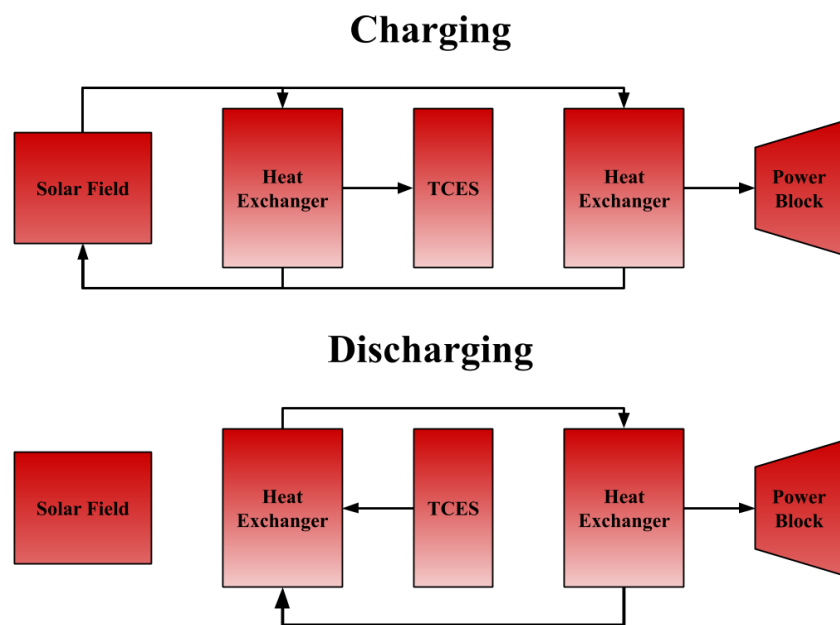


Figure 5 - Parallel configuration of CSP with TCES while charging and discharging adapted Strohle et al. [11]

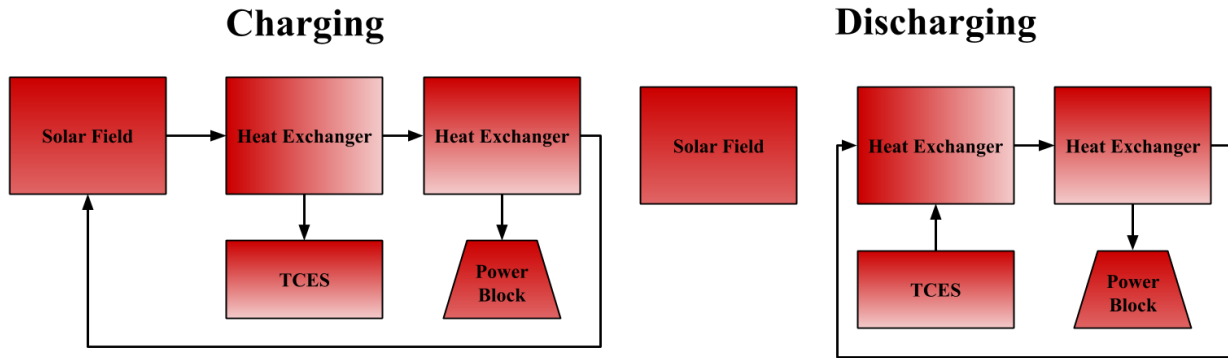


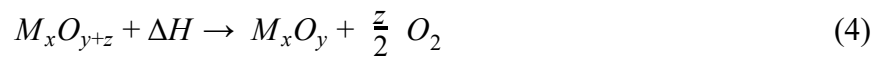
Figure 6 - Serial configuration of CSP with TCES while charging and discharging adapted Strohle et al. [11]

Metal Oxide TCES

Implementation of TCES with CSP can provide consistent energy supply from a renewable energy source but is underdeveloped when compared to other renewable energy processes like PV and wind. However, processes like wind and PV cannot store energy economically as they are currently limited to technologies such as batteries which are expensive and have low energy densities. Depending on the operating temperatures, TCES allows for energy storage using processes such as the dehydration of salt hydrates or metal hydrates, the decarboxylation of metal carbonates, and the redox reaction of metal oxides [12].

Dehydration and decarboxylation often require storage of H_2O and CO_2 respectively that is generated while charging for later discharge [12]. This additional material storage can increase the capital and operating costs of the process. On the other hand, with proper pressure and temperature control, metal oxides have the ability to source and generate O_2 in air [12]. This ability means there is no need to store the working fluid as air can be used when charging as O_2 is generated and discharging when O_2 is consumed.

The first step in the redox reaction of a metal oxide occurs when the sun inputs energy and be can be described as,



The second step in the redox reaction of a metal oxide occurs when there is no energy input from the sun and can be described as,



Most of these reactions occur in the range of 700 to 1100 °C and are heavily dependent on the partial pressure of O_2 as seen in Figure 7. By leveraging the impact of pressure and temperature

on the redox reaction of a metal oxide, energy can be stored while charging and generated while discharging using air as the primary working fluid for both cases.

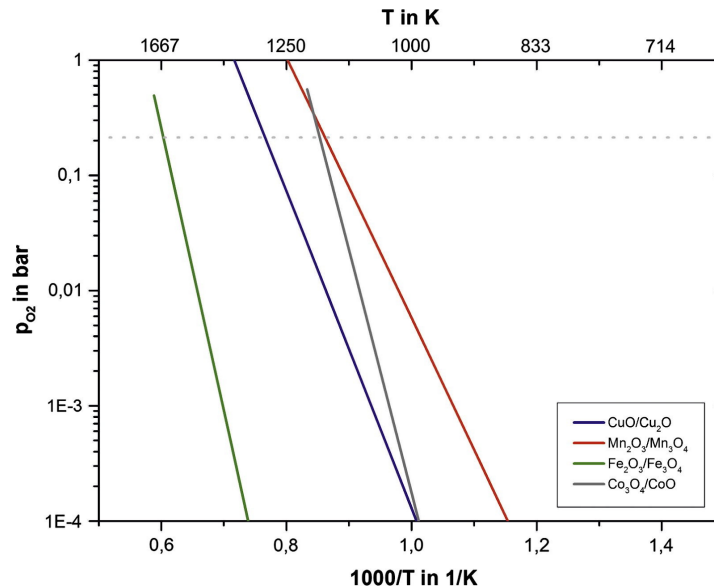


Figure 7 - Partial pressure of oxygen impacting the reaction temperature of various metal oxide TCES material from Block and Schmucker [13]

By using air as the working fluid throughout the redox reaction, a mixture between the general Brayton Cycle and combustion can be used to generate electricity. Because air can be used for both TCES and electricity generation, a secondary heating fluid such as Rankine Cycle is not required for the main power production but may be advantageous for heat recovery downstream. This limits the number of heat exchangers and working fluids required for the process which can decrease the capital and operating costs.

CSP and TCES in a Brayton Cycle

CSP allows for high temperatures up to 1600 K to be reached for a pressured air receiver which is approaching temperatures that challenge metallurgical requirements [14]. Being able to reach these high temperatures allows for CSP to act as the heater or combustion chamber in a Brayton Cycle. Previous implementations of CSP and TCES into a Brayton Cycle have been achieved with a two step TCES cycle as shown in Figure 8. In this approach, the TCES material cycles between hot and cold storage tanks and reacts with the compressed gas to heat the stream before entering the turbine. This system uses a CoO/Co₃O₄ cycle for the TCES demonstrating the ability of the metal oxide reaction occurring in air. This approach was able to reach cycle efficiencies between approximately 26% at 5 bar to 44% at 30 bar [15]. These efficiencies are higher than that of commercially available solar PV and the storage allows for production of electricity to occur when there is no energy input from the sun.

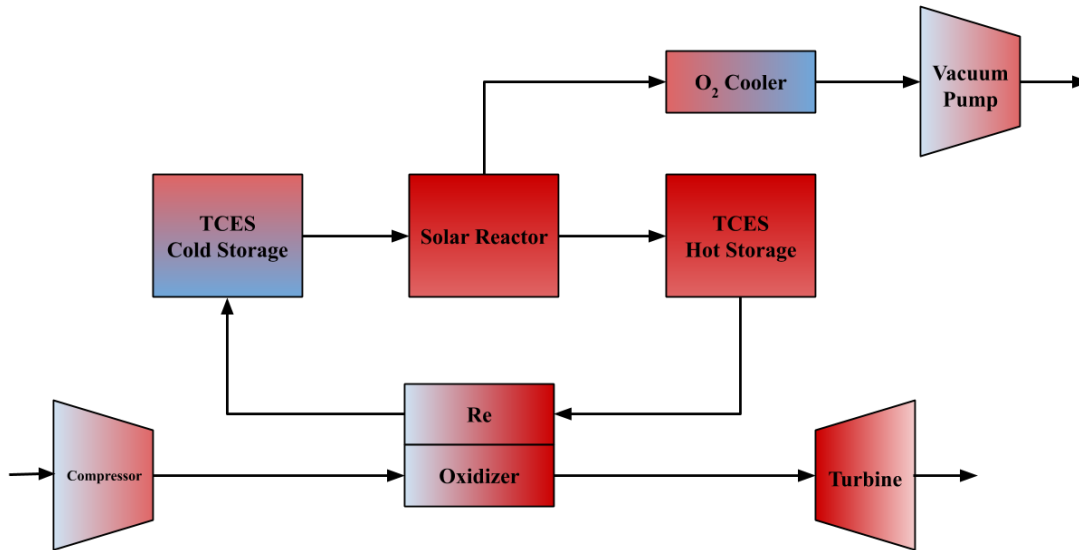


Figure 8 - Serial configuration of a cycling TCES system adapted from Schardier et al. [15]–[17]

While this approach has achieved relatively high cycle efficiency, the movement of solids increases the frequency of the reaction which could lead to high rates of material degradation. Additionally, the system requires a vacuum pump and cooler for the O_2 from the charging of the TCES. The vacuum pump increases the required work input of the system which decreases the cycle efficiency. Additionally, the cooler takes a high temperature gas stream from the reactor to atmospheric conditions. This loss of high temperature energy will decrease the cycle efficiency. Additionally, this system follows the model of a serial configuration for TCES so the Re-Oxidizer is best implemented as a falling particle reactor. As a result, there will need to be additional equipment for moving the TCES material between the cold and hot storage. Overall, the TCES cycle illustrated here acts as more of a separate cycle with the Re-Oxidizer acting as a heat exchanger for the air stream.

Barium Oxide-Peroxide Energy Storage

With the idea of using a metal oxide with air for TCES, the exact metal oxide must be chosen. There are many different metal oxide systems that can be used for TCES but choosing one to operate in air in a parallel configuration requires careful selection. While previous attempts have used the $\text{CoO}/\text{Co}_3\text{O}_4$ cycle, the $\text{Mn}_2\text{O}_3/\text{Mn}_2\text{O}_4$, $\text{CuO}/\text{Cu}_2\text{O}$, and BaO_2/BaO have been identified as candidates for TCES as well as shown in Figure 9 [18].

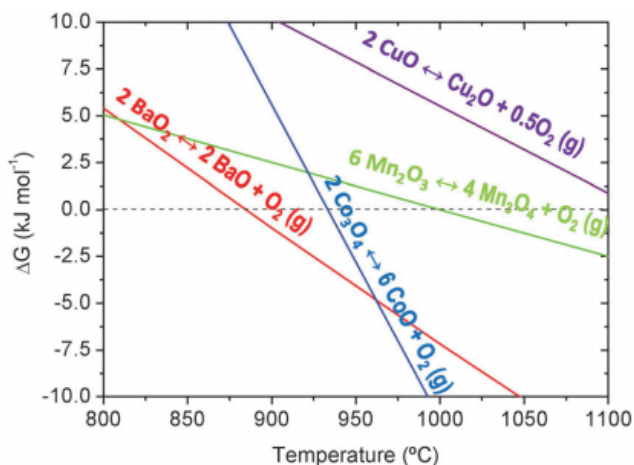


Figure 9 - Various metal oxide TCES systems from Carillo et al. [18]

A study into the feasibility of using the BaO_2/BaO system has been examined and demonstrated long-term reversibility of the redox reaction and operates at more moderate temperatures than other materials proposed for TCES [18]. Additionally, the BaO_2/BaO system has a high energy density of 390 kJ/kg and has been demonstrated using commercially available materials [18].

The BaO_2/BaO system has been used in the past to produce relatively pure O_2 from air by manipulating the redox cycle to act as a separation unit. By leveraging the effect of temperature and pressure on the system, as seen in Figure 10, in the late 1800s it was used to create O_2 purities up to 96% from air [19]. This demonstration of the success of this system along with the high energy associated with it makes the BaO_2/BaO system seen in Equation 6 a prime candidate for TCES operating in air in a parallel configuration.



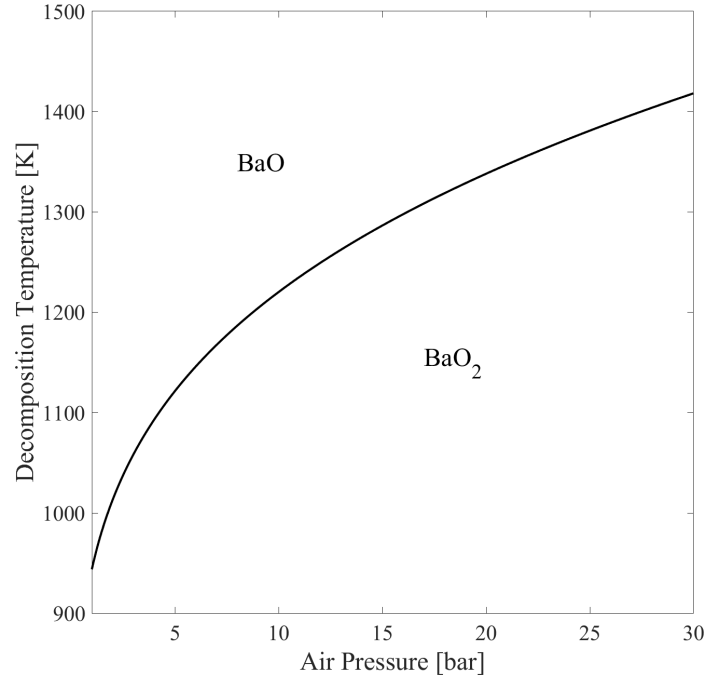


Figure 10 - Decomposition temperature dependence on the air pressure adapted from Fahim and Ford [20]

Approach

Based upon the observations of parallel and serial configurations, the effect of the pressure and temperature on the BaO_2/BaO system, and the success of a serial configuration of TCES in a Brayton Cycle, a parallel configuration must be explored. The BaO_2/BaO system is more favorable in a packed bed rather than a fluidized bed because it is a soft material. A proposed system for charging and discharging of a parallel configuration of TCES implemented into a Brayton Cycle is illustrated in Figures 11-12.

The central ideas for this approach is to limit the use of heat exchangers and working fluids in the process by utilizing air as the primary working fluid when both charging and discharging. In this parallel configuration the compressed air is heated by a solar field before splitting into the TCES for storage and the gas turbine for electricity production. A secondary Rankine Cycle can be added for additional heat recovery.

The air does not cycle through the system back to the compressor making it more analogous to combustion than a Brayton Cycle so the outlets of the system must be as close to atmospheric conditions as possible when exiting the system. This further indicates the need for the Rankine Cycle by taking the leftover energy from the outlet of the gas turbine and the TCES. Based on this, the outlet from the gas turbine and the TCES are set to 1.5 bar and air leaving the system

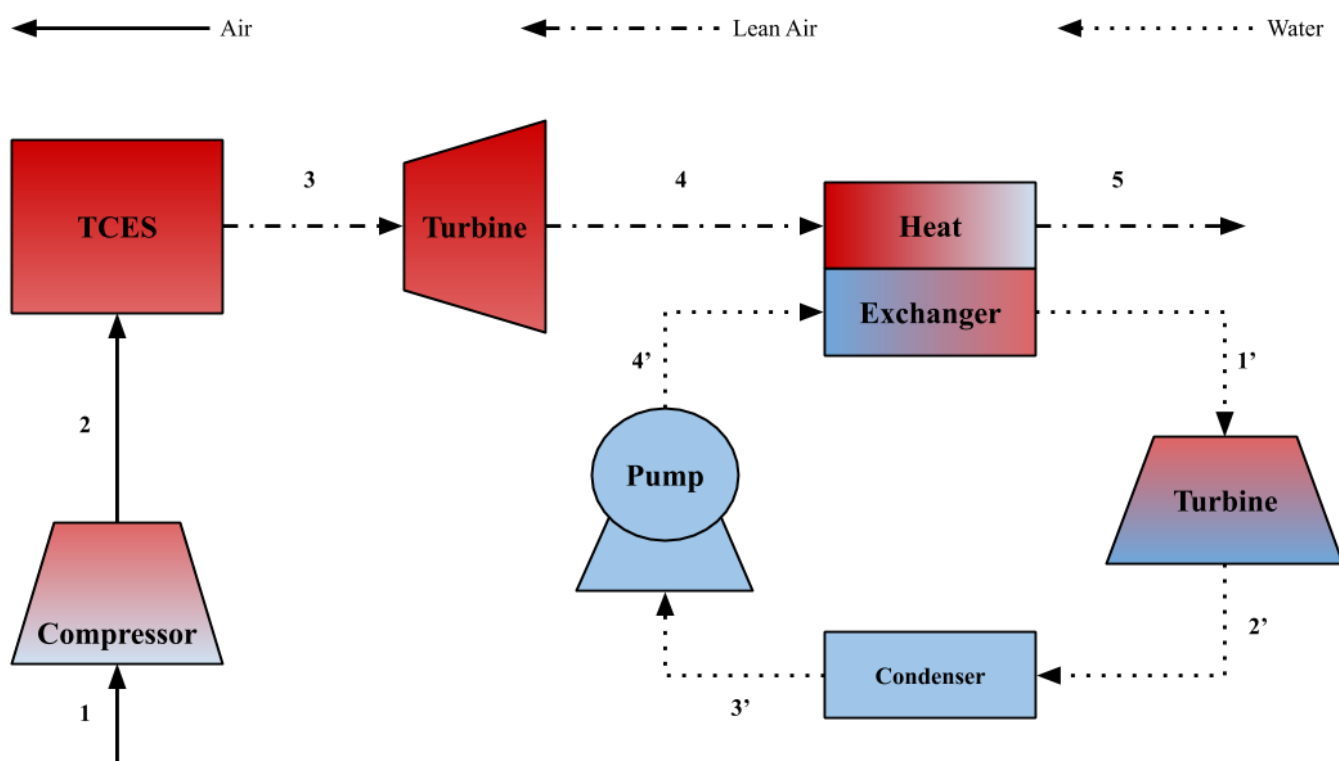


Figure 12 - Block diagram of the system with a single stage compressor while discharging

For discharge in Figure 12, the TCES bed must heat the air stream from the compressor outlet (Stream 1) before entering the turbine (Stream 3). To accomplish this, the outlet of TCES bed is limited by the decomposition temperature of the BaO_2 . The outlet temperature of the TCES bed was set to 90% of the decomposition temperature of BaO_2 at the outlet pressure of the bed. While the pressure drop of the TCES bed while charging depends on the compression ratio, the pressure drop of the TCES bed while discharging will be set to 1 bar. This means the air will only pass through one of the TCES bed reactors at a time while discharging and the compression ratio while discharging will be 1 more than the compression ratio while charging.

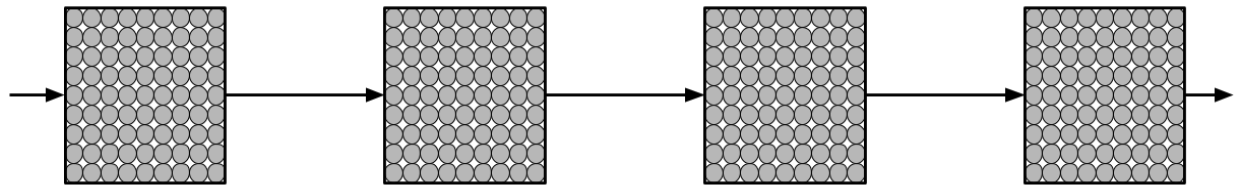


Figure 13 - TCES serial bed while charging

To test the viability of this system, MATLAB was used to model a 50 MW_e plant at a variety of charging compression ratios. There is approximately 8 hours of peak sun in some areas; meaning there needs to be 16 hours of off sun storage to produce electricity continuously.

Key Equations

Brayton Cycle

Brayton Cycle analysis and equations are the main components of the modeling of this system. The first step for both charging and discharging is the compression of air from atmospheric pressure. The outlet temperature and specific work of the compressor for a gas turbine can be determined from Equation 7 and 8 respectively. The key parameters for these equations are the isentropic efficiency of the compressor, η_C , the compression ratio, P_{r_c} , and the heat capacity ratio, k . The isentropic efficiency of the compressor was chosen to be 0.8 as a typical value. The heat capacity ratio depends on the outlet temperature of the compressor, so a while loop was used in MATLAB to converge the outlet temperature and heat capacity ratio.

$$T_{C_{out}} = T_{C_{in}} + \frac{T_{C_{in}}}{\eta_C} (P_{r_c}^{\frac{k-1}{k}} - 1) \quad (7)$$

$$W_C = \frac{C_p T_{C_{in}}}{\eta_C} (P_{r_c}^{\frac{k-1}{k}} - 1) \quad (8)$$

For the gas turbine, similar equations are used to determine the outlet temperature and specific work for the turbine in Equation 9 and 10, respectively. Again, key parameters for these equations are the isentropic efficiency of the turbine, η_t , the pressure ratio of the turbine, P_{r_t} , and the heat capacity ratio, k . The same while loop method was used for convergence of the outlet temperature and heat capacity ratio.

$$T_{t_{out}} = T_{t_{in}} + T_{t_{in}} \eta_e (P_{r_t}^{\frac{k-1}{k}} - 1) \quad (9)$$

$$W_t = C_p T_{t_{in}} \eta_e (P_{r_t}^{\frac{k-1}{k}} - 1) \quad (10)$$

For analysis of the efficiency of a Brayton Cycle, the thermal input to net power out of the cycle determined by Equation 11. A higher thermal to electricity efficiency is desirable as it will decrease the required thermal input for a set power production.

$$\eta = \frac{W_{net}}{Q_{in}} = \frac{|W_t + W_C|}{Q_{in}} \quad (11)$$

Rankine Cycle

The Rankine Cycle used in the system is put in to recover as much of the thermal energy as reasonably possible. To model the Rankine Cycle using the chosen high and low pressures of 7.5 bar and 1 bar, the specific pump input and turbine output must be determined using Equation 12 and 13, respectively. Where the isentropic efficiency for the pump and the steam turbine are both 0.8.

$$W_{sc} = \eta_{sc} (h_{l,sub}|_{P_{high}} - h_{l,sat}|_{P_{low}}) \quad (12)$$

$$W_{st} = \frac{1}{\eta_{st}} (h_{mix}|_{P_{low}} - h_{vap}|_{P_{high}}) \quad (13)$$

The required flow rate in the Rankine Cycle will depend on the energy transfer from the air stream to the water. To evaluate this the energy required to vaporize the water can be determined from Equation 14 to solve for a water to air molar flow rate.

$$Q_{air \rightarrow RC} = h_{vap}|_{P_{low}} - h_{l,sub}|_{P_{high}} \quad (14)$$

Cycle

To evaluate the performance of an entire charging to discharging cycle, the total energy produced while charging and discharging must be determined. This is accomplished by multiplying the specific net work by the required air flow to meet and time for the charging and discharging periods separately. Then the overall solar to electric efficiency can be determined from Equation 15.

$$\eta_{cycle} = \frac{W_{net,ch} t_{on,sun} + W_{net,dis} t_{off,sun}}{Q_{CSP} t_{on,sun}} \quad (15)$$

Results and Discussion

Charging

While the TCES bed is charging, it is important to determine how much of the high temperature air from the CSP goes to the turbine for electricity production and how much goes to the TCES bed for energy storage. To do this, the thermal to electric conversion efficiency of the system while discharging must be determined. This is accomplished by first modeling the 16 hours discharge to determine the amount of BaO that needs to be stored while charging. Once this is determined, the required air flow to the TCES bed while charging can be determined. Then, the air flow to the turbine can be determined in order to reach the target power production of 50 MW_e.

With all of the required parameters determined, the 8 hour charging period can be analyzed. First, the TCES air splitting ratio was determined and illustrated in Figure 14. The air splitting ratio decreases as the charging compression ratio increases. With any Brayton Cycle, the efficiency of the process increases with the compression ratio. For this system it means less BaO will have to be stored at higher compression ratios because the discharge process will be more energy efficient. At a charging compression of 10.7, the solar array reaches the maximum pressurized air CSP receiver temperature of 1600 K [14], [21], [22]. At his compression ratio, the air splitting ratio reaches a minimum of 0.49.

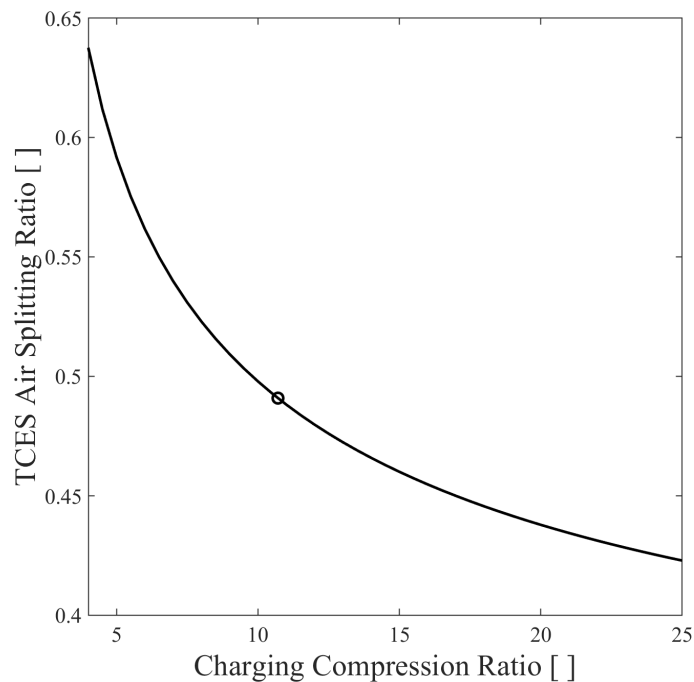


Figure 14 - TCES air splitting ratio while charging for the system with a single stage compressor with the circle denoting the operation at the maximum receiver temperature

This observation is further exemplified by the amount of BaO required for storage and the corresponding required solar array area displayed in Figure 15. At the maximum receiver temperature, the minimum solar array area is 2.6 km^2 assuming a 1000 W/m^2 input from the sun and the minimum amount of BaO storage required is 8400 m^3 for 0% porosity at the maximum receiver temperature. To put the required storage volume into perspective, a CSP system rated for the same electricity production using molten salt for energy storage can have a total volume for cold and hot storage tanks of $60,000 \text{ m}^3$ for 9 hours of storage [23].

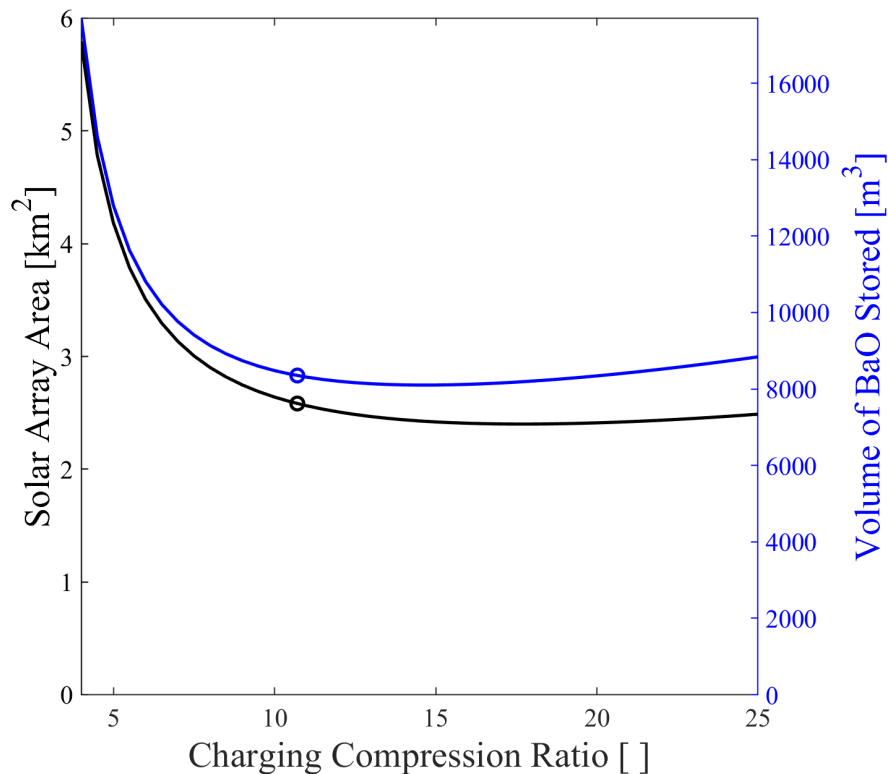


Figure 15 - Required solar array area and storage volume of BaO for the system with a single stage compressor. The circle is operation at the maximum receiver temperature

Discharging

The discharge parameters of required BaO storage and air flow are determined by the parameters for charging. To analyze the discharging phase, the TCES thermal input to electricity efficiency can be determined as seen in Figure 16. The TCES thermal input to electricity efficiency increases with the charging compression ratio initially before beginning to decrease. This does follow typical Brayton Cycle trends where the efficiency increases with the compression ratio.

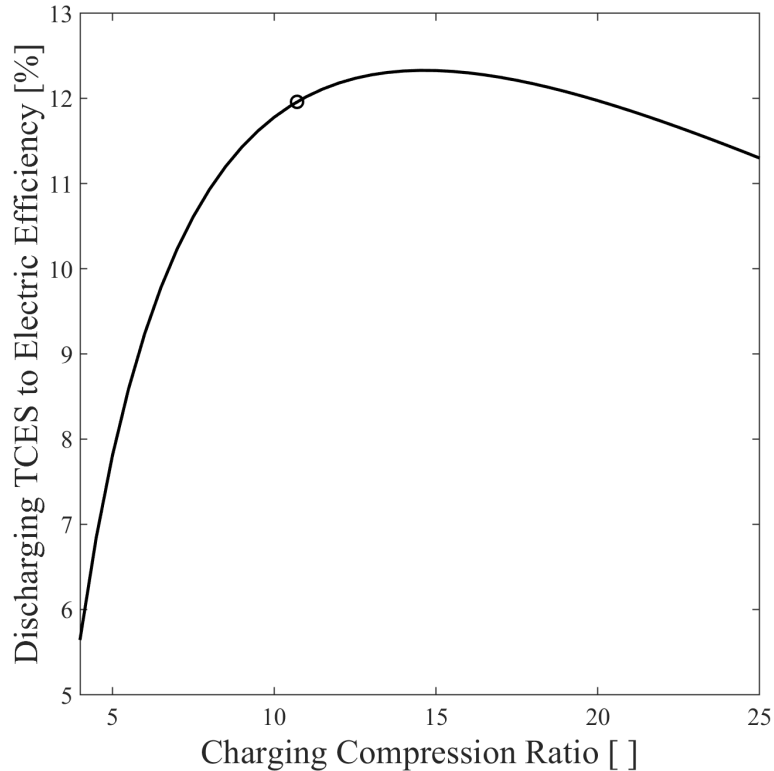


Figure 16 - Discharge TCES to electric conversion efficiency using a single stage compressor. The circle is operation at the maximum receiver temperature

To understand why the efficiency of the system is decreasing at high compression ratios, the outlet temperature of the compressor and the TCES bed is plotted in Figure 17. The temperature difference between the two decreases at higher compression ratios meaning the thermal input from the TCES bed is not enough to make the energy input required by the compressor less than the energy output from the main turbine.

This is illustrated in Figure 18 where the energy input from the compressor is equal to the energy output from the turbine at a compression ratio of 41. At compression ratios higher than 41, the Rankine Cycle is able to produce enough energy to overcome this until the compression ratio reaches 147 and the total energy input is less than total energy output.

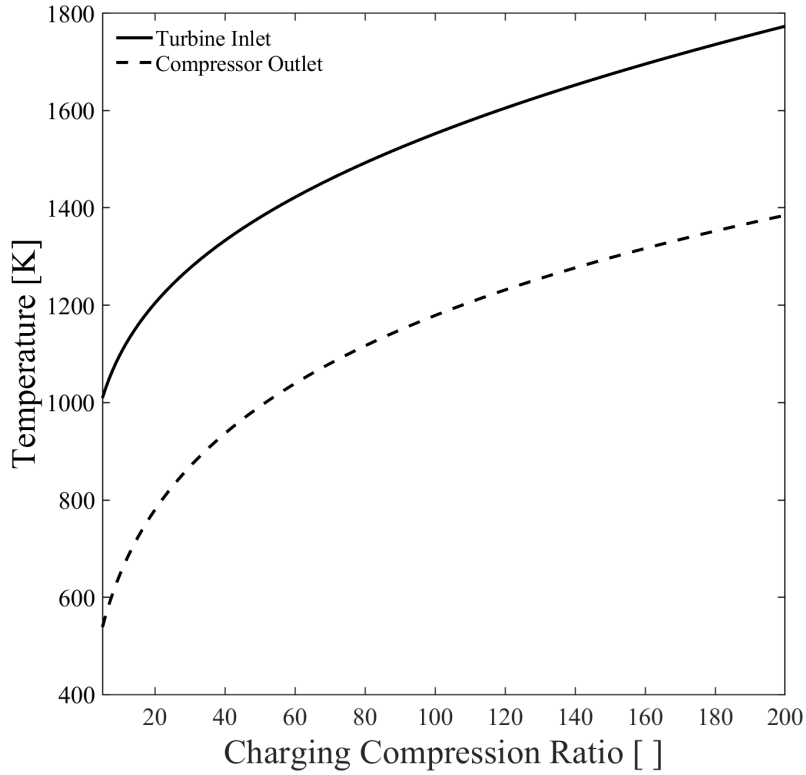


Figure 17 - Turbine inlet and compressor outlet temperatures while discharging using single stage compressor

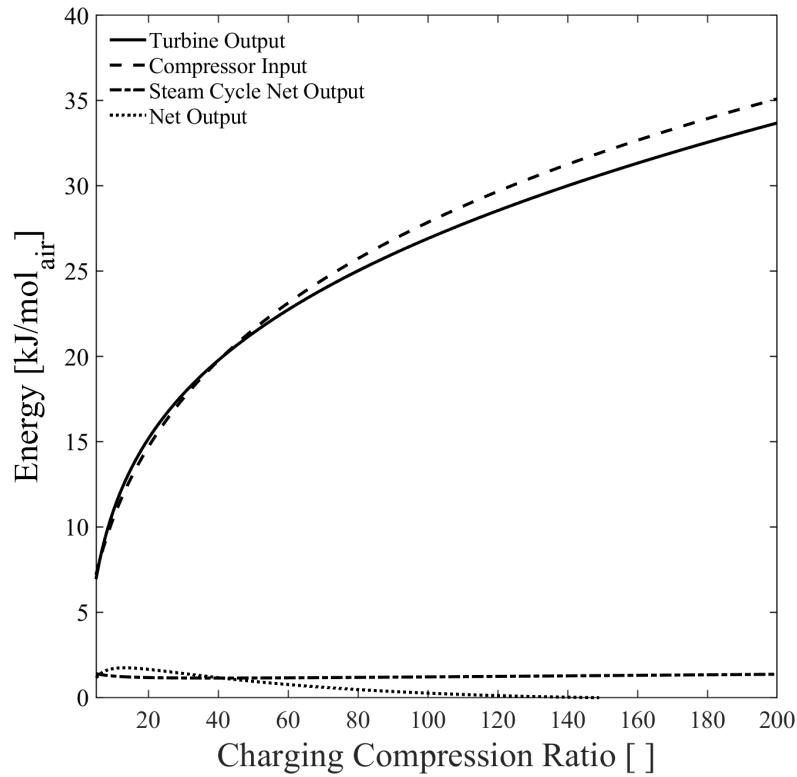


Figure 18 - Discharge specific energy streams using a single stage compressor

Complete Cycle

With both the charging and discharging periods modeled and analyzed, the complete charging to discharging cycle can be analyzed. First, the overall, solar thermal to electric efficiency can be determined and is illustrated in Figure 19. The solar thermal to electric efficiency initially and 5.8% at the maximum receiver temperature. However, the solar to electric efficiency reaches a maximum of 6.3% at a compression ratio 17.5 before beginning to decrease. This can be explained by the trend observed in the discharge efficiency that did not follow traditional Brayton Cycle trends.

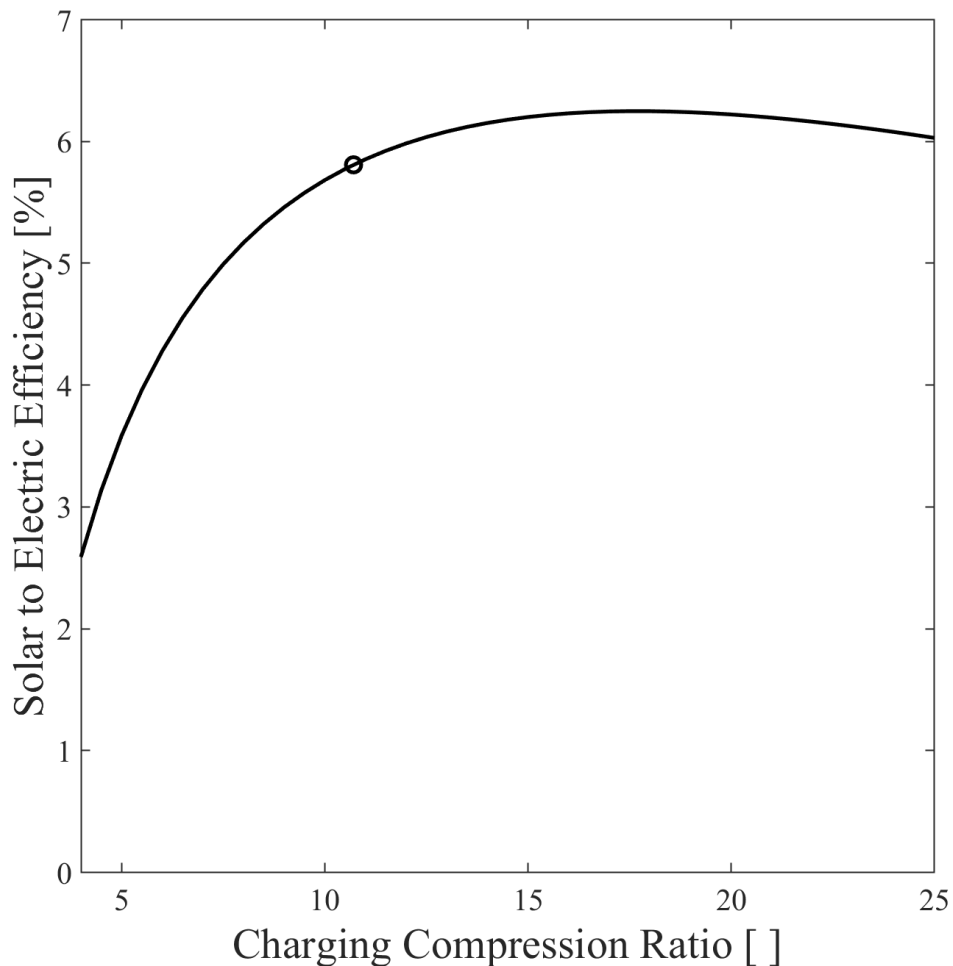


Figure 19 - Solar to electric conversion efficiency of the system using a single stage compressor. The circle is operation at the maximum receiver temperature

To understand the required scale of the system, the required air flow and the water to air molar ratio is illustrated in Figure 20 for both charging and discharging. The required air flow for both

charging and discharging follows the same trend of the solar to electric efficiency. The large difference between the required flows for charging and discharging is accounted for by the charging phase having to store the required energy for discharge. The difference between the charging and discharging required air flow rates decreases with the charging compression ratio as the discharging becomes more efficient until the discharge efficiency begins to decrease at the higher compression ratios. Additionally, the water to air molar ratio is lower when discharging than when charging because charging operates at higher temperatures than discharging.

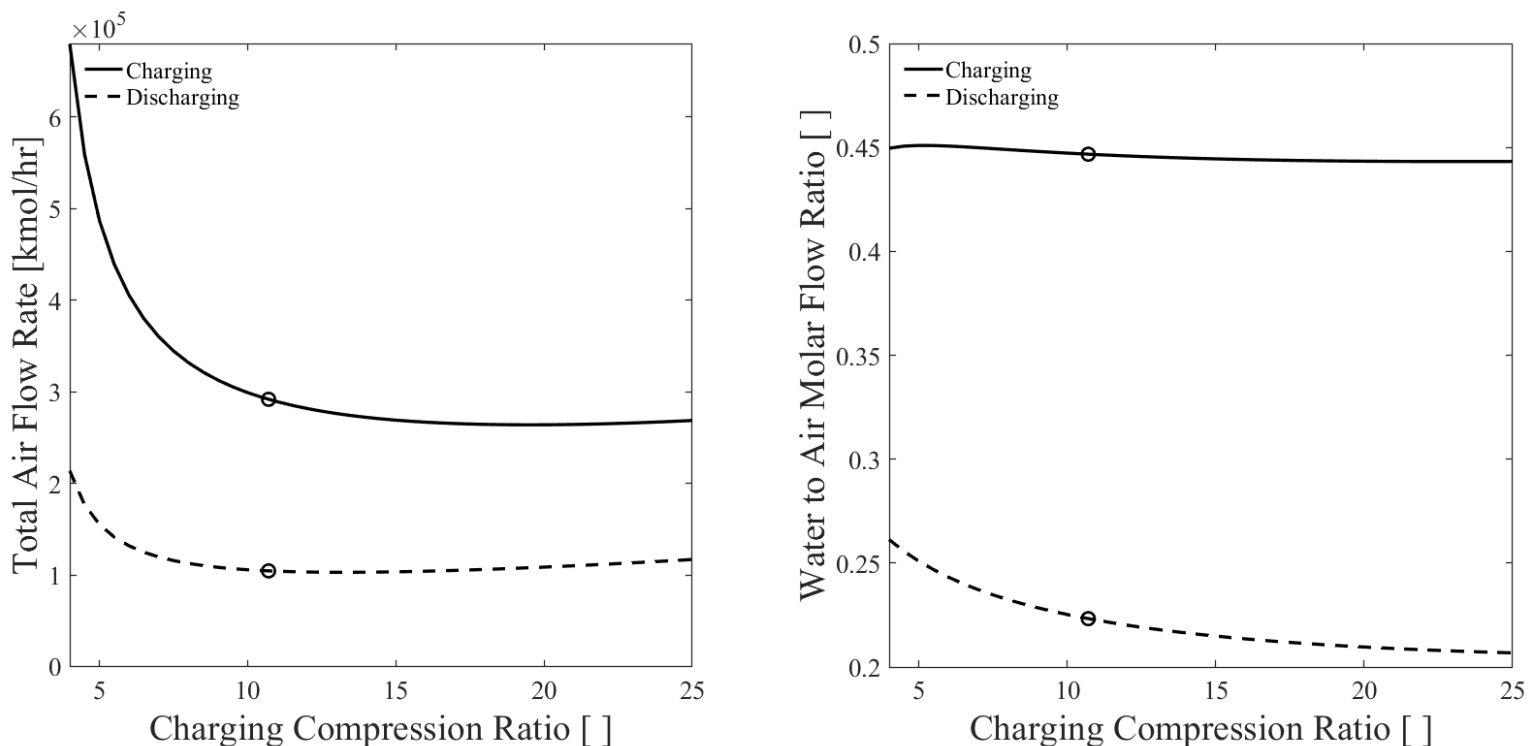


Figure 20 - Required air flows and water to air molar flow ratios for charging and discharging using a single stage compressor. The circle is operation at the maximum receiver temperature.

Other CSP systems with TES, have solar thermal to electric efficiencies up to approximately 40% so it is on the lower end of typical efficiencies [24]. Despite this, considering this was the first iteration of this system, there are areas that could be improved upon. Primarily, this simple modeling does not take into account the additional benefit associated with the BaO_2/BaO system to store and release sensible energy as the energy from the reaction. Additionally, the compression and turbine expansion were completed in a single stage. Previous work found the addition of a two-stage compressor with an intercooler had a higher solar to electric efficiency than a single stage compressor for a CSP plant without energy storage [10]. Implementation of a multistage compressor for this system with energy storage could lead to higher solar to electric

efficiencies even though it would increase the required temperature increase by the TCES bed while discharging.

These hypotheses were tested by implementing a two-stage compressor with an intercooler that cooled the gas stream to 323 K. Additionally, the CSP was varied to heat the gas stream to 15% above the decomposition temperature rather than 30% more. This was done by maximizing the solar to electric conversion at the maximum receiver temperature. The results of these changes are illustrated in Figure 21. The efficiency at the maximum receiver temperature is now 7.6% and the system now exhibits the traditional Brayton Cycle behavior where the efficiency of the system increases with the compression ratio. This change improved the efficiency at the maximum receiver temperature by 30% relative to the single stage compressor case.

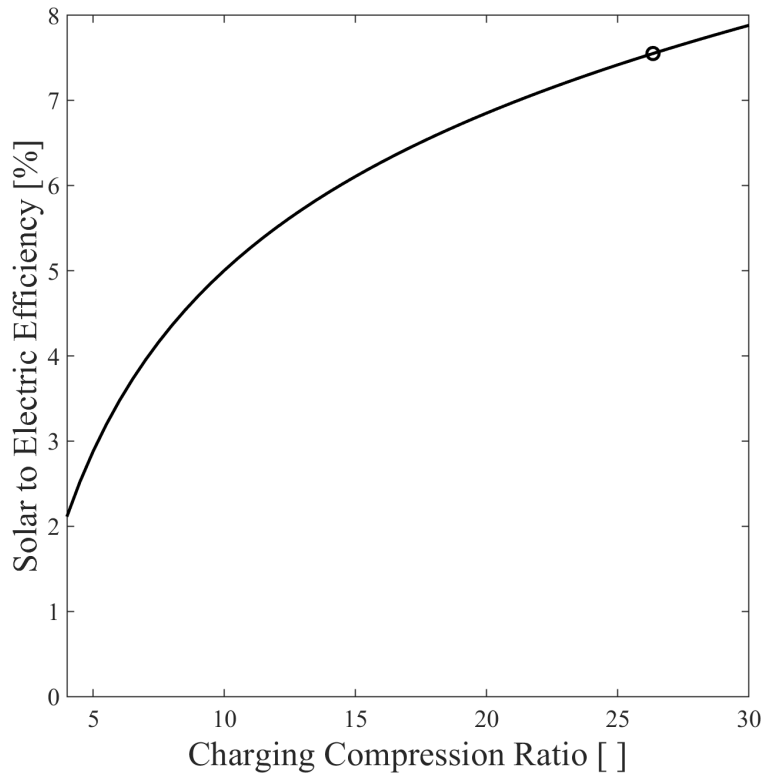


Figure 21 - Solar to electric efficiency of the system using a two-stage compression with an intercooler. The circle is operation at the maximum receiver temperature.

The improvements in the cycle efficiency can be further exemplified by the amount of BaO required for storage and the corresponding required solar array area displayed in Figure 22. At the maximum receiver temperature, the minimum solar array area is now 2.0 km² and the minimum amount of BaO storage required is 5200 m³ at the maximum receiver temperature. This a 23% decrease in the solar array area and a 38% decrease in the required storage volume.

Additionally, the discharging TCES to electric efficiency at the maximum receiver temperature increased from 12% to 18%; an improvement of 60%.

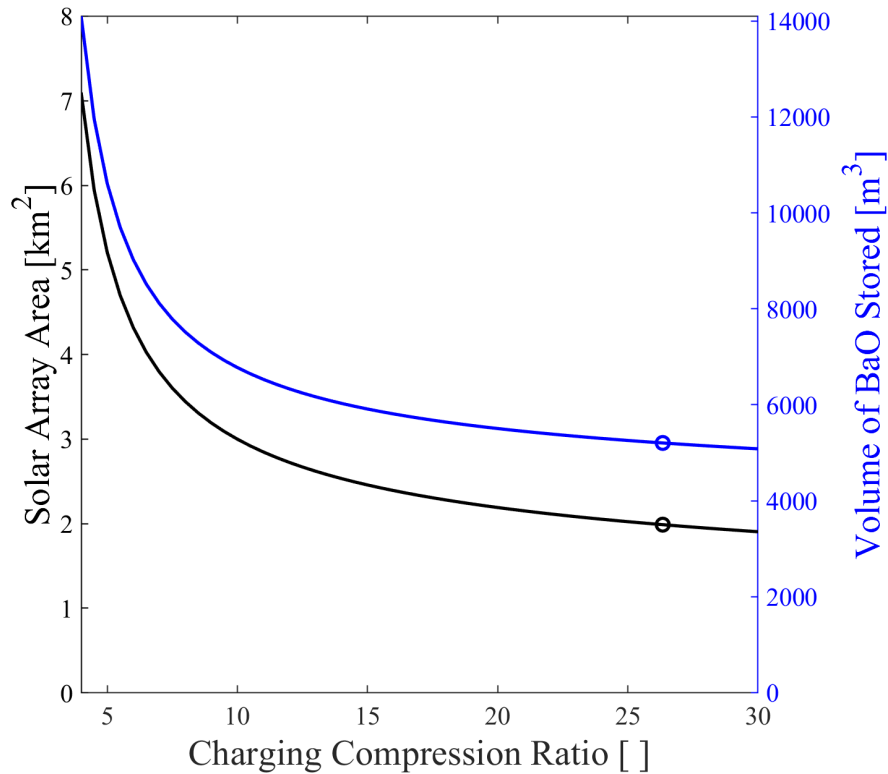


Figure 22 - Required solar array area and storage volume of BaO for the system with a two-stage compressor with an intercooler. The circle is operation at the maximum receiver temperature.

To understand the sensitivity of the system on the turbine. The outlet pressure of the turbine was lowered from 1.5 bar to 1 bar. This may not seem like a significant change, but it had a significant effect on the system with a two-stage compressor. Figure 23 shows the solar to electric efficiency of the system with 11.9% at the maximum receiver temperature. This is a 57% increase from the base two-stage compressor case, and more than double the efficiency of the single stage compressor case.

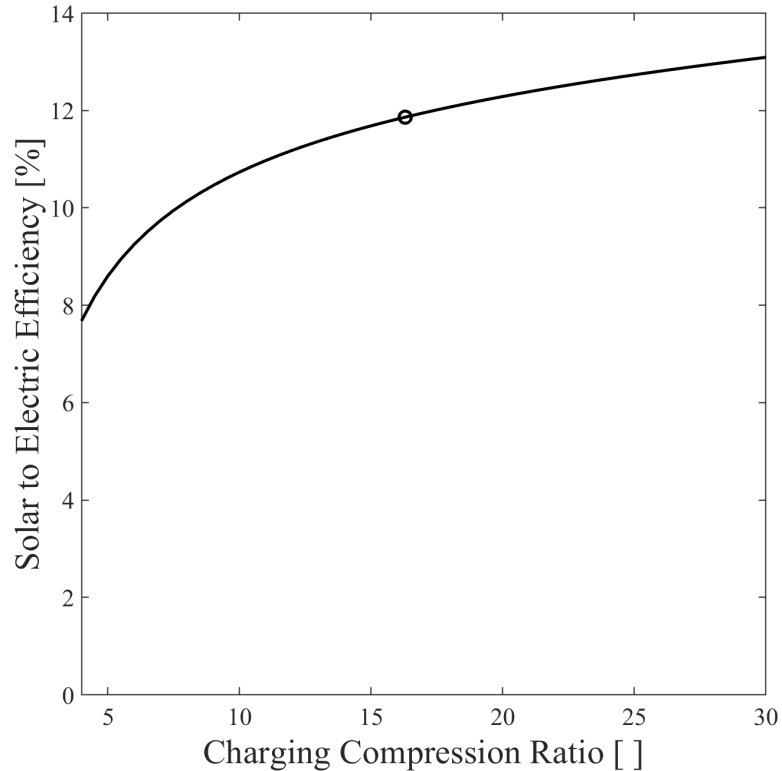


Figure 23 - Solar to electric efficiency of the system with a decreased turbine outlet pressure of 1 bar for the system with a two-stage compressor. The circle is operation at the maximum receiver temperature.

The sensitivity of the system to the turbine outlet pressure and the use of the two-stage compressor suggest there ways to improve the efficiency of the system. Methods to increase the efficiency, however, would add complexity to the system that was initially designed for simplicity. Whether or not the increased efficiency would be beneficial for the process in terms of the cost of the electricity produced would require detailed economic analysis. However, based on the solar to electric efficiency achieved by these systems, there may be some value in the simplistic design.

HYSYS Validation

To validate the performance of the MATLAB modeling, the base system with a single compressor while discharging was modeled in HYSYS in Figure 24. A NRTL-SRK model was chosen and the same operating inlet and outlet pressures and temperatures were set. Additionally, the isentropic efficiencies of the turbines and compressors/pumps were set to the same value of 0.8.

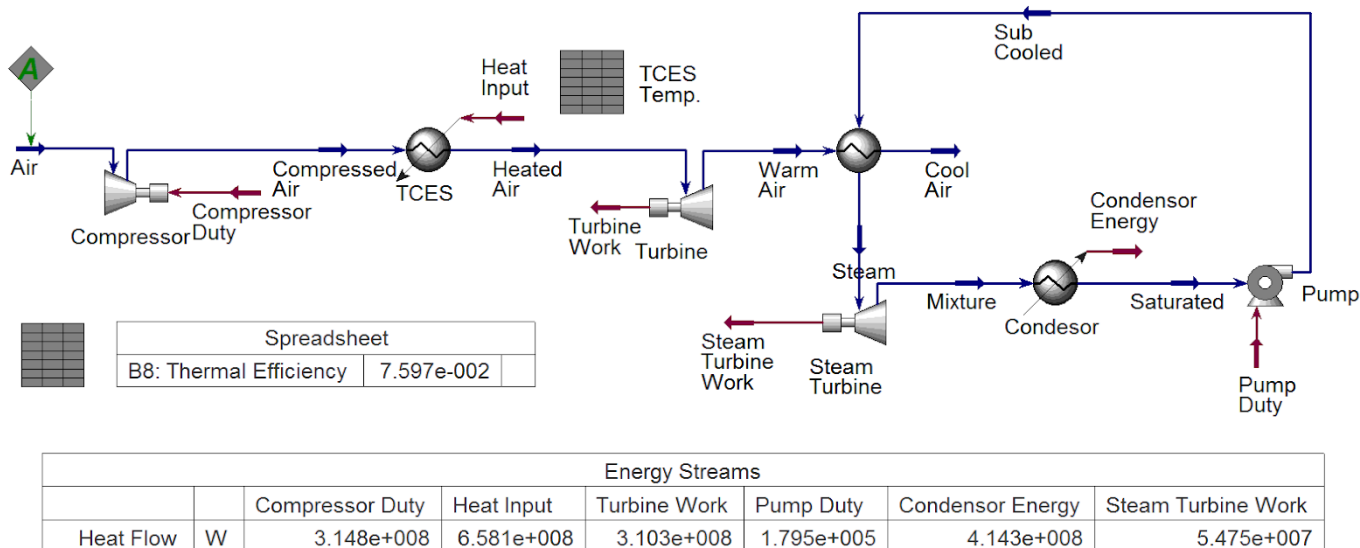


Figure 24 - HYSYS model of the system while discharging at a charging compression ratio of 6.

To compare the MATLAB model with the HYSYS model, the TCES to electricity conversion efficiency and the required flow to produce 50 MW_e is plotted in Figure 25. There is close agreement between the HYSYS model and the MATLAB model at lower compression ratios but decreases at higher compression ratios. The average error for the efficiency between the HYSYS model and MATLAB is 3.1% and is 1.4% for the air flow. The average between these two is 2.2%. The close agreement between HYSYS model and MATLAB model validates the MATLAB model's performance.

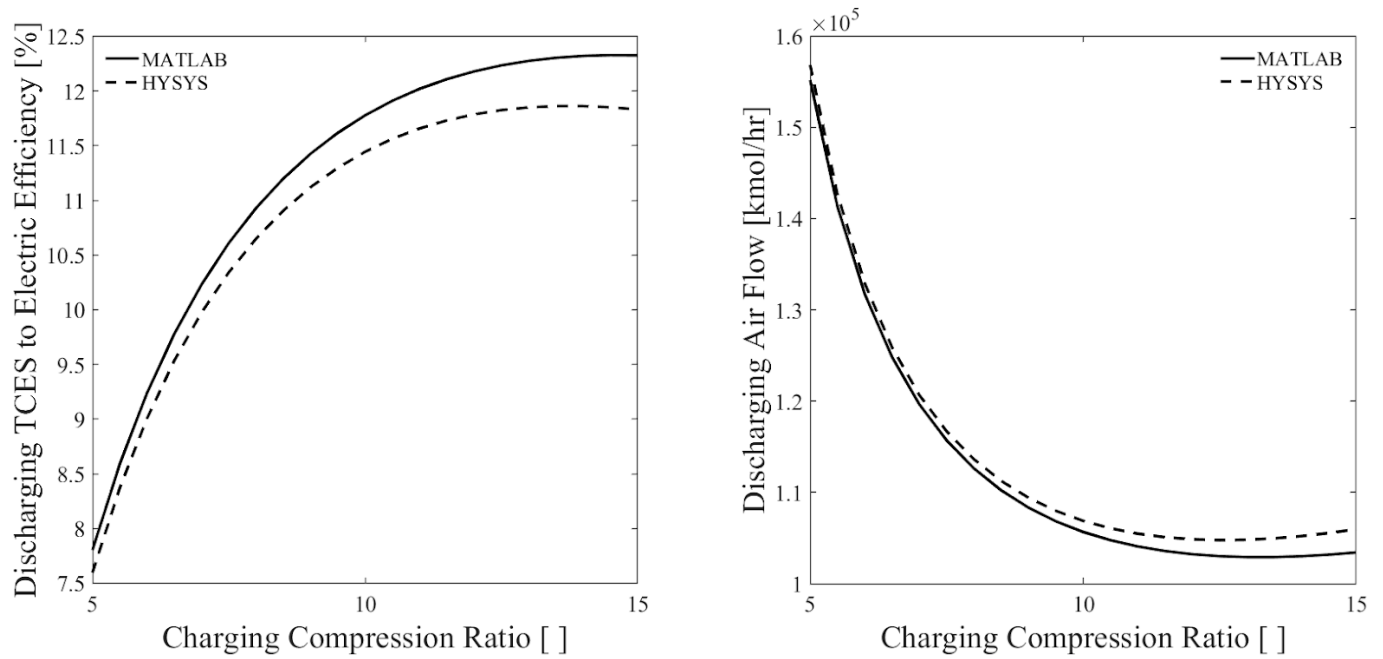


Figure 25 - Comparison of TCES to electric efficiency and air flow rate for MATLAB and HYSYS.

Conclusion

This system was modelled to determine if the simplicity of the proposed design would greatly impact performance. The key benefit of this design will be the potential capital costs associated with it. This first look into the system did not address this benefit. A potential downside of this approach is the TCES is stored and operated in pressure vessels which could decrease the capital cost benefit of the simple design.

While the solar to electric efficiency of the base was quite low, the few simple changes to the system were able to increase the efficiency to 10-12%. While current commercially available PV is higher than this, the system can produce electricity beyond peak sun hours through the night. This benefit makes this system competitive as it can be a producer of baseload power.

Additionally, the decreased solid cycling of the TCES material when compared to the serial configuration by Schardier et al is another key benefit of this system. The decreased solid cycling has the potential to decrease the required amount of fresh material over time as issues such as sintering will be decreased. This means operational costs of the system could be decreased.

Altogether, the system modeled in this work has the potential to be a beneficial configuration of TCES into a Brayton Cycle despite the challenges it faces with increased compressor duty caused by the pressure drop of the TCES bed. Further work into the economic benefit of this is required to make more definitive statements about the final practicality of the system.

Future Work

This is the first iteration of the system and it has many areas of improvement. It has already been demonstrated how a more efficient two-stage compressor has been able to improve the overall cycle solar to electric efficiency. For the power block, there has been work on using a recuperator instead of a Rankine Cycle following the turbine outlet which could be applied to this system [21]. The recuperator could be implemented into the system in two different ways: for the TCES outlet while charging and for turbine outlet while charging and discharging. Although this system was initially designed to limit the number of heat exchangers, the outlet stream of the TCES while charging is still at high temperatures can be used to heat the air from the compressor before it enters the solar field. This has the potential to decrease the required solar input which would increase the cycle efficiency. Other areas of improvement could be the use of multiple TCES and sensible materials for storage. The concept of consecutive reactions has been demonstrated previously and could lead to higher thermal efficiencies [25].

References

- [1] “World Energy Balances 2019 Overview.pdf.” .
- [2] D. Mills, “Advances in solar thermal electricity technology,” *Sol. Energy*, vol. 76, no. 1–3, pp. 19–31, Jan. 2004, doi: 10.1016/S0038-092X(03)00102-6.
- [3] G. Alva, L. Liu, X. Huang, and G. Fang, “Thermal energy storage materials and systems for solar energy applications,” *Renew. Sustain. Energy Rev.*, vol. 68, pp. 693–706, Feb. 2017, doi: 10.1016/j.rser.2016.10.021.
- [4] G. Alva, Y. Lin, and G. Fang, “An overview of thermal energy storage systems,” *Energy*, vol. 144, pp. 341–378, Feb. 2018, doi: 10.1016/j.energy.2017.12.037.
- [5] C. Prieto, P. Cooper, A. I. Fernández, and L. F. Cabeza, “Review of technology: Thermochemical energy storage for concentrated solar power plants,” *Renew. Sustain. Energy Rev.*, vol. 60, pp. 909–929, Jul. 2016, doi: 10.1016/j.rser.2015.12.364.
- [6] H. L. Zhang, J. Baeyens, J. Degève, and G. Cacères, “Concentrated solar power plants: Review and design methodology,” *Renew. Sustain. Energy Rev.*, vol. 22, pp. 466–481, Jun. 2013, doi: 10.1016/j.rser.2013.01.032.
- [7] Y. Lin, Y. Jia, G. Alva, and G. Fang, “Review on thermal conductivity enhancement, thermal properties and applications of phase change materials in thermal energy storage,” *Renew. Sustain. Energy Rev.*, vol. 82, pp. 2730–2742, Feb. 2018, doi: 10.1016/j.rser.2017.10.002.
- [8] R. Chacartegui, A. Alovio, C. Ortiz, J. M. Valverde, V. Verda, and J. A. Becerra, “Thermochemical energy storage of concentrated solar power by integration of the calcium looping process and a CO₂ power cycle,” *Appl. Energy*, vol. 173, pp. 589–605, Jul. 2016, doi: 10.1016/j.apenergy.2016.04.053.
- [9] C. Ortiz, R. Chacartegui, J. M. Valverde, A. Alovio, and J. A. Becerra, “Power cycles integration in concentrated solar power plants with energy storage based on calcium looping,” *Energy Convers. Manag.*, vol. 149, pp. 815–829, Oct. 2017, doi: 10.1016/j.enconman.2017.03.029.
- [10] X. Wang, Q. Liu, J. Lei, W. Han, and H. Jin, “Investigation of thermodynamic performances for two-stage recompression supercritical CO₂ Brayton cycle with high temperature thermal energy storage system,” *Energy Convers. Manag.*, vol. 165, pp. 477–487, Jun. 2018, doi: 10.1016/j.enconman.2018.03.068.
- [11] S. Ströhle, A. Haselbacher, Z. R. Jovanovic, and A. Steinfeld, “The effect of the gas–solid contacting pattern in a high-temperature thermochemical energy storage on the performance of a concentrated solar power plant,” *Energy Environ. Sci.*, vol. 9, no. 4, pp. 1375–1389, 2016, doi: 10.1039/C5EE03204K.
- [12] H. B. Dizaji and H. Hosseini, “A review of material screening in pure and mixed-metal oxide thermochemical energy storage (TCES) systems for concentrated solar power (CSP) applications,” *Renew. Sustain. Energy Rev.*, vol. 98, pp. 9–26, Dec. 2018, doi: 10.1016/j.rser.2018.09.004.
- [13] T. Block and M. Schmücker, “Metal oxides for thermochemical energy storage: A comparison of several metal oxide systems,” *Sol. Energy*, vol. 126, pp. 195–207, Mar. 2016, doi: 10.1016/j.solener.2015.12.032.
- [14] I. Hischer, P. Leumann, and A. Steinfeld, “Experimental and Numerical Analyses of a

- Pressurized Air Receiver for Solar-Driven Gas Turbines,” *J. Sol. Energy Eng.*, vol. 134, no. 2, p. 021003, May 2012, doi: 10.1115/1.4005446.
- [15] A. J. Schrader, A. P. Muroyama, and P. G. Loutzenhiser, “Solar electricity via an Air Brayton cycle with an integrated two-step thermochemical cycle for heat storage based on Co₃O₄/CoO redox reactions: Thermodynamic analysis,” *Sol. Energy*, vol. 118, pp. 485–495, Aug. 2015, doi: 10.1016/j.solener.2015.05.045.
- [16] A. J. Schrader, G. De Dominicis, G. L. Schieber, and P. G. Loutzenhiser, “Solar electricity via an Air Brayton cycle with an integrated two-step thermochemical cycle for heat storage based on Co₃O₄/CoO redox reactions III: Solar thermochemical reactor design and modeling,” *Sol. Energy*, vol. 150, pp. 584–595, Jul. 2017, doi: 10.1016/j.solener.2017.05.003.
- [17] H. E. Bush and P. G. Loutzenhiser, “Solar electricity via an Air Brayton cycle with an integrated two-step thermochemical cycle for heat storage based on Fe₂O₃/Fe₃O₄ redox reactions: Thermodynamic and kinetic analyses,” *Sol. Energy*, vol. 174, pp. 617–627, Nov. 2018, doi: 10.1016/j.solener.2018.09.043.
- [18] A. J. Carrillo, D. Sastre, D. P. Serrano, P. Pizarro, and J. M. Coronado, “Revisiting the BaO₂/BaO redox cycle for solar thermochemical energy storage,” *Phys. Chem. Chem. Phys.*, vol. 18, no. 11, pp. 8039–8048, 2016, doi: 10.1039/C5CP07777J.
- [19] W. B. Jensen, “The Origin of the Brin Process for the Manufacture of Oxygen,” *J. Chem. Educ.*, vol. 86, no. 11, p. 1266, Nov. 2009, doi: 10.1021/ed086p1266.
- [20] M. A. Fahim and J. D. Ford, “Energy storage using the BaO₂ ⇌ BaO reaction cycle,” *Chem. Eng. J.*, vol. 27, no. 1, pp. 21–28, Aug. 1983, doi: 10.1016/0300-9467(83)80042-2.
- [21] W. G. Le Roux, T. Bello-Ochende, and J. P. Meyer, “The efficiency of an open-cavity tubular solar receiver for a small-scale solar thermal Brayton cycle,” *Energy Convers. Manag.*, vol. 84, pp. 457–470, Aug. 2014, doi: 10.1016/j.enconman.2014.04.048.
- [22] H. von Storch, M. Roeb, H. Stadler, C. Sattler, and B. Hoffschmidt, “Available online Efficiency potential of indirectly heated solar reforming with different types of solar air receivers,” *Appl. Therm. Eng.*, vol. 92, pp. 202–209, Jan. 2016, doi: 10.1016/j.applthermaleng.2015.09.065.
- [23] U. Herrmann, B. Kelly, and H. Price, “Two-tank molten salt storage for parabolic trough solar power plants,” *Energy*, vol. 29, no. 5–6, pp. 883–893, Apr. 2004, doi: 10.1016/S0360-5442(03)00193-2.
- [24] U. Pelay, L. Luo, Y. Fan, D. Stitou, and M. Rood, “Thermal energy storage systems for concentrated solar power plants,” *Renew. Sustain. Energy Rev.*, vol. 79, pp. 82–100, Nov. 2017, doi: 10.1016/j.rser.2017.03.139.
- [25] L. F. Cabeza *et al.*, “Thermochemical energy storage by consecutive reactions for higher efficient concentrated solar power plants (CSP): Proof of concept,” *Appl. Energy*, vol. 185, pp. 836–845, Jan. 2017, doi: 10.1016/j.apenergy.2016.10.093.

Appendix

Key MATLAB Codes

Functions

```
function Del_h = idealairenthalpychange(T_out, T_in)

%This function is for calculating the enthalpy change associated with a temperature difference of air
%This uses the ideal heat capacity of air

R = 8.314; % [J/molK]

A = 3.355; B = 0.575*10^(-3); C = 0; D = -0.016*10^(-5); E = 0; % constants

T_min = 298; T_max = 2000; % [K] temperature range

if T_in < T_min || T_out < T_min || T_in > T_max || T_out > T_max %Determines if the model is appropriate
    error('Temperatures are out of range') %Will stop the program if the model is not appropriate
end

h = @(T) R * (A * T + (1/2) * B * T.^2 + (1/3) * C * T.^3 - D * T.^(-1) + (1/4) * E * T.^4); % [J/mol]
Calculates the enthalpy at T with T = 0 as a reference

Del_h = h(T_out) - h(T_in); % [J/mol] Calculates the enthalpy change across the temperature range

end
```

Published with MATLAB® R2020a

```
function [T_f, P_out, W_C] = compressor(T_in, P_in, P_r_C, eff_C)

%This functions determines the compressor output temperature

R = 8.314; % [J/mol-K] gas constant

A = 3.355; B = 0.575*10^(-3); C = 0; D = -0.016*10^(-5); E = 0; % constants for C_P and C_v

C_p = @(T) R * (A + B .* T + C * T.^2 + D * T.^(-2) + E * T.^3); % [J/mol-K] Ideal heat capacity of air at
constant pressure

C_v = @(T) R * (A + B .* T + C * T.^2 + D * T.^(-2) + E * T.^3) - R; % [J/mol-K] Ideal heat capacity of air at
constant volume

T_out = T_in + 300; % [K] temporary temperature to be used for calculation

C_p_bar = integral(C_p, T_in, T_out)/(T_out - T_in); % [J/mol-K] Calculates the average C_p over the temperature
range

C_v_bar = integral(C_v, T_in, T_out)/(T_out - T_in); % [J/mol-K] Calculates the average C_v over the temperature
```

```

range

k_bar = C_p_bar / C_v_bar; % [ ]Calculates the average heat capacity ratio over the temperature range

P_out = P_r_C * P_in; % [Pa] output pressure

T_out = T_in + T_in/eff_C * ((P_out/P_in)^((k_bar - 1)/k_bar) - 1); % [K] initial output temperature

err = 100; %random initial error

while err > 10^(-10)

    C_p_bar = integral(C_p, T_in, T_out)/(T_out - T_in); % [J/mol-K] Calculates the average C_p over the
    temperature range

    C_v_bar = integral(C_v, T_in, T_out)/(T_out - T_in); % [J/mol-K] Calculates the average C_v over the
    temperature range

    k_bar = C_p_bar / C_v_bar; % [J/mol-K] Calculates the average heat capacity ratio over the temperature range

    T_out_new = T_in + T_in/eff_C * ((P_out/P_in)^((k_bar - 1)/k_bar) - 1); % [K] output temperature

    err = (T_out_new - T_out)/T_out_new; % [ ]relative error

    T_out = T_out_new; % [K] renaming

end

W = C_p_bar * T_in / eff_C * ((P_out/P_in)^((k_bar - 1)/k_bar) - 1); % {J/mol] work input

T_f = T_out; % [K] output of function
W_C = W; % [J/mol] output of function

end

```

Published with MATLAB® R2020a

```

function [T_f, P_f, Q_in] = powertower(T_in, P_in)

a = 4170; b = 3.74; % constants for decomposition temperature

T = @(P_O2) -a./(log10(P_O2/101325)- b); % [K] decomposition temperature

P_O2 = 0.21 * P_in; % [Pa] pressure of O_2

T_out = T(P_O2) * 1.3; % [K] output temperature with extra heating

if T_out < T_in % determines in compressor outlet temperature is higher

    error('Temperature cross - powertower') % Will stop the program if energy is not increased with power tower

end

P_out = P_in; % [Pa] outlet pressure of power tower

T_f = T_out; % [K] output of function

```

```

P_f = P_out; % [Pa] output of function

Q_in = abs(idealairenthalpychange(T_in, T_f)); % [J/mol-air] energy required from the sun the heat the air
stream

end

```

Published with MATLAB® R2020a

```

function [T_f, P_f, W_t] = turbine(T_in,P_in, eff_t,P_r_t)

P_out = P_in * P_r_t; % [Pa] output pressure

R = 8.314; % [J/mol-K] gas constant

A = 3.355; B = 0.575*10^(-3); C = 0; D = -0.016*10^(-5); E = 0; % constants for air C_P and C_v

C_p = @(T) R * (A + B .* T + C * T.^2 + D * T.^(-2) + E * T.^3); % [J/mol-K] Ideal heat capacity of air at
constant pressure

C_v = @(T) R * (A + B .* T + C * T.^2 + D * T.^(-2) + E * T.^3) - R; % [J/mol-K] Ideal heat capacity of air at
constant volume

T_out = T_in - 300; % [K] temporary temperature to be used for calculation

C_p_bar = integral(C_p, T_in, T_out)/(T_out - T_in); % [J/mol-K] Calculates the average C_p over the temperature
range

C_v_bar = integral(C_v, T_in, T_out)/(T_out - T_in); % [J/mol-K] Calculates the average C_v over the temperature
range

k_bar = C_p_bar / C_v_bar; % [ ] Calculates the average heat capacity ratio over the temperature range

T_out = T_in + T_in * eff_t * ((P_out/P_in)^((k_bar - 1)/k_bar) - 1); % [K] initial output temperature

err = 100; %random initial error

while err > 10^(-10)

    C_p_bar = integral(C_p, T_in, T_out)/(T_out - T_in); % [J/mol-K] Calculates the average C_p over the
temperature range

    C_v_bar = integral(C_v, T_in, T_out)/(T_out - T_in); % [J/mol-K] Calculates the average C_v over the
temperature range

    k_bar = C_p_bar / C_v_bar; % [ ] Calculates the average heat capacity ratio over the temperature range

    T_out_new = T_in + T_in * eff_t * ((P_out/P_in)^((k_bar - 1)/k_bar) - 1); % [K] output temperature

    err = (T_out_new - T_out)/T_out_new; % relative error

    T_out = T_out_new; % [K] renaming

end

W = C_p_bar * T_in * eff_t * ((P_out/P_in)^((k_bar - 1)/k_bar) - 1); % {J/mol} work output

```

```

T_f = T_out; % [K] output of function
P_f = P_out; % [Pa] output of function
W_t = W; % [J/mol] [output of function

end

```

Published with MATLAB® R2020a

```

function [n_react, n_air_dis, Q_TCES] = TCESDischarge(P_r_C_ch, W_desired, off_sun)

T_C_in = 298; % [K] compressor inlet temperature during discharge
P_C_in = 101325; % [Pa] compressor inlet pressure during charging
eff_C = 0.8; % [ ] isentropic efficiency of the compressor
P_r_C_dis = P_r_C_ch + 1; % [ ] compression ratio during discharge
[T_C_out_dis, P_C_out_dis, W_C_dis] = compressor(T_C_in, P_C_in, P_r_C_dis, eff_C);
[T_t_in_dis, P_t_in_dis, Q_TCES] = TCES_bed_dis(T_C_out_dis, P_C_out_dis);
P_r_t_dis = 1.5 / (P_t_in_dis/101325); % [ ] pressure ratio of turbine during discharge
eff_t = 0.8; % [ ] isentropic efficiency of the main turbine during discharge
[T_t_out_dis, P_t_out_dis, W_t_dis] = turbine(T_t_in_dis, P_t_in_dis, eff_t, P_r_t_dis);
eff_st = 0.8; % [ ] isentropic efficiency of the steam turbine during discharge
eff_sc = 0.8; % [ ] isentropic efficiency of the steam compressor during discharge
[T_out, P_out, W_st_dis, W_sc_dis, Q_transf_dis, Q_s_cond_dis, mol_ratio_dis] = steam_turbine(T_t_out_dis,
P_t_out_dis, eff_st, eff_sc);
W_net_dis = W_t_dis + W_C_dis + W_st_dis + W_sc_dis; % {J/mol-air} net work during discharge
if W_net_dis > 0 %Determines if net work is producing electricity
    error('W_net_dis>0') %Will stop the program if electricity is not produced
end
n_air_dis = W_desired / (W_net_dis); % [mol-air/s] required air flow during discharge
if n_air_dis < 0 %Determines if there is negative air flow
    error('Negative Flow - TCESDischarge n_air_dis') %Will stop the program if there is a negative flow
end
del_h = 77.3 * 10^3; % [J/mol-BaO] enthalpy of decomposition
n_react = n_air_dis * off_sun * 60 * 60 * Q_TCES / del_h; % [mol-BaO] required moles of BaO that needs to be
stored

```

```
end
```

Published with MATLAB® R2020a

```
function [T_out, P_out, Q_rel] = TCES_bed_dis(T_in, P_in)

a = 4170; b = 3.74; % constants for decomp temp

T = @(P_O2) -a./(log10(P_O2/101325)- b); % [K] temperature of decomposition

P_out = P_in - 101325; % [Pa] output pressure from the TCES bed during discharge

P_O2 = 0.21 * P_out; % [Pa] partial pressure of O2 at TCES outlet during discharge

T_out = T(P_O2) * 0.9; % [K] output temperature of TCES bed during discharge

Q_rel = abs(idealairenthalpychange(T_in, T_out)); % [J/mol-air] energy released from TCES bed during discharge

end
```

Published with MATLAB® R2020a

```
function [T_out, P_out, n_air_TCES_ch] = TCESCharge(n_react, T_in, on_sun)

del_h = 77.3 * 10^3; % [J/mol-BaO]

a = 4170; b = 3.74; % constant for decomp temp

T = @(P_O2) -a./(log10(P_O2/101325)- b); % [K] decomp temperature

P_out = 1.5 * 101325; % [Pa] outlet pressure

P_O2 = 0.21 * P_out; % [Pa] outlet partial oxygen pressure

T_out = T(P_O2); % [K] outlet temperature

h_transf = abs(idealairenthalpychange(T_out, T_in)); % [J/mol-air] energy transfer from the air to the TCES bed
during charging

n_air_TCES_ch = n_react * del_h / on_sun / 60 / 60 / h_transf; % [mol-air/s] required air flow to TCES during
charging

if n_air_TCES_ch < 0 %Determines if the model there is negative flow

    error('Negative Flow - TCESCharge n_air_TCES_ch') % Will stop the program if there is a negative flow

end

end
```

Published with MATLAB® R2020a

```

function [n_air_t_ch, split_ratio] = Turbine_Charging(T_TCES_out_ch, n_air_TCES_ch, W_desired, W_t_ch, W_C_ch,
T_t_out_ch, P_t_out_ch, P_TCES_out_ch)

eff_st = 0.8; % [ ] isentropic efficiencies of the turbine in the steam cycle

eff_sc = 0.8; % [ ] isentropic efficiencies of the pump in the steam cycle

[T_out, P_out, W_st_1, W_sc_1, Q_transf_1, Q_s_cond_1, mol_ratio_1] = steam_turbine(T_TCES_out_ch,
P_TCES_out_ch, eff_st, eff_sc);

W_1_net = W_st_1 + W_sc_1 + W_C_ch; % [J/mol-air-TCES] per mol air work from in going through TCES

W_1_net_out = W_1_net * n_air_TCES_ch; % [W] net work out from air going through the TCES

W_2_net_out = W_desired - W_1_net_out ; % [W] required total work for air going out of power tower to the
turbine to the steam loop

[T_out, P_out, W_st_2, W_sc_2, Q_transf_2, Q_s_cond_2, mol_ratio_2] = steam_turbine(T_t_out_ch, P_t_out_ch,
eff_st, eff_sc);

W_2_net = W_t_ch + W_C_ch + W_st_2 + W_sc_2; % [J/mol-air-turbine] net work from air going through the turbine

n_air_t_ch = W_2_net_out / W_2_net; % required air flow through the turbine

if n_air_t_ch < 0 %Determines if the flow is negative

    error('Negative Flow - Turbine_Charging n_air_t_ch') % Will stop the program if the model if a negative
flow occurs

end

split_ratio = n_air_TCES_ch/ (n_air_t_ch + n_air_TCES_ch); % splitting ratio of air to TCES during charging

end

```

Published with MATLAB® R2020a

```

function [T_out, P_out, W_st, W_sc, Q_transf, Q_s_cond, mol_ratio] = steam_turbine(T_in, P_in, eff_st, eff_sc)

T_out = 175 + 273; % [K] air output temperature

P_out = P_in; % [Pa] output pressure

Q_transf = idealairenthalpychange(T_in, T_out); % [J/mol-air] energy transferred from the air to the steam cycle

h_3 = 50.030 * 1000; % [J/mol] enthalpy of saturated steam at 7.5 [bar]

s_3 = 118.63; % [J/mol-K] entropy of saturated steam at 7.5 [bar]

s_4 = s_3; % [J/mol-K] entropy of the ideal turbine outlet at 1 [bar]

s_4_liq = 23.470; % [J/mol-K] entropy of saturated liquid at 1 [bar]

s_4_vap = 132.57; % [J/mol-K] entropy of saturated steam at 1 [bar]

```

```

x_4 = (s_4 - s_4_liq)/(s_4_vap - s_4_liq); % [ ] vapor quality of the turbine outlet

h_4_vap = 48.190 * 1000; % [J/mol] enthalpy of saturated steam at 1 [bar]

h_4_liq = 7.5214 * 1000; % [J/mol] enthalpy of saturated liquid at 1 [bar]

h_4 = x_4 * h_4_vap + (1 - x_4) * h_4_liq; % [J/mol] enthalpy of the turbine outlet at 1 [bar]

h_1 = h_4_liq; % [J/mol] enthalpy of the condensed water at 1 [bar]

s_1 = s_4_liq; % [J/mol-K] entropy of the condensed water at 1 [bar]

s_2 = s_1; % [J/mol-K] entropy of the compressed water at 7.5 [bar]

h_2 = 7.5385 * 1000; % [J/mol] enthalpy of the compressed water at 7.5 [bar]

mol_ratio = Q_transf/(h_3 - h_2); % [ ] mol ratio of water to air

W_st_ideal = mol_ratio * (h_4 - h_3); % [J/mol-air] ideal work done by the steam turbine

W_st = W_st_ideal * eff_st; % [J/mol-air] work output by the steam turbine

Q_s_cond = mol_ratio * (h_1 - h_4); % [J/mol-air] energy required to condense steam

W_sc_ideal = mol_ratio * (h_2 - h_1); % [J/mol-air] ideal work required for the compressor

W_sc = W_sc_ideal / eff_sc; % [J/mol-air] real work required for the compressor

end

```

Published with MATLAB® R2020a

```

function T_mix = air_mixing(T_1, n_1, T_2, n_2)

Q_1 = @(T_mix) n_1 * idealairenthalpychange(T_mix, T_1); % [J/s] energy difference for stream 1

Q_2 = @(T_mix) n_2 * idealairenthalpychange(T_mix, T_2); % [J/s] energy difference for stream 2

f = @(T_mix) Q_1(T_mix) + Q_2(T_mix); % [J/s] sum of the energy differences for stream 1 and 2

T_guess = (n_1 * T_1 + n_2 * T_2) / (n_1 + n_2); % [K] initial estimate for mixing temperature

T_mix = fzero(f, T_guess); % [K] mixing temperature

end

```

Published with MATLAB® R2020a

Complete Cycle

```

close all; clear all; clc;

%% determining charging parameters %%
T_C_in = 298; % [K] atmospheric temperature
P_C_in = 101325; % [Pa] atmospheric pressure
eff_C = 0.8; % [ ] isentropic efficiency of the compressor
P_r_C_ch = 5:0.5:15; %[ ] charging compression ratio
W_desired = zeros(1, length(P_r_C_ch)) - 50 * 10^(6); % [W] capacity of power plant
off_sun = 16; % [hr]
on_sun = 8; % [hr]
T_max = 1600; % [K] max CSP temperature
Q_sun = 1000; % [W/m^2] energy from the sun

% compression %
for i = 1:length(P_r_C_ch)

    [T_C_out_ch(i), P_C_out_ch(i), W_C_ch(i)] = compressor(T_C_in, P_C_in, P_r_C_ch(i), eff_C);

end

% CSP %
for i = 1:length(P_r_C_ch)

    [T_t_in_ch(i), P_t_in_ch(i), Q_in_ch(i)] = powertower(T_C_out_ch(i), P_C_out_ch(i));

end

% calculating required storage for discharge %
P_r_t_ch = 1.5 ./ (P_r_C_ch);
for i = 1:length(P_r_C_ch)

    [n_react(i), n_air_dis(i), Q_TCES_dis(i)] = TCESDischarge(P_r_C_ch(i), W_desired(i), off_sun);

end

```

```

% determining the air flow required to TCES during charging %
for i = 1:length(P_r_C_ch)

    [T_TCES_out_ch(i), P_TCES_out_ch(i), n_air_TCES_ch(i)] = TCESCharge(n_react(i), T_t_in_ch(i), on_sun);

end

% determining energy from main turbine %
eff_t = 0.8;

for i = 1:length(P_r_C_ch)

    [T_t_out_ch(i), P_t_out_ch(i), W_t_ch(i)] = turbine(T_t_in_ch(i), P_t_in_ch(i), eff_t, P_r_t_ch(i));

end

% determining the air flow to the turbine %
for i = 1:length(P_r_C_ch)

    [n_air_t_ch(i), split_ratio(i)] = Turbine_Charging(T_TCES_out_ch(i), n_air_TCES_ch(i), W_desired(i),
W_t_ch(i), W_C_ch(i), T_t_out_ch(i), P_t_out_ch(i), P_TCES_out_ch(i));

end

% % charging % %
T_C_in = 298; % [K] atmospheric temperature
P_C_in = 101325; % [Pa] atmospheric pressure to compressor
eff_C = 0.8; % [ ] isentropic efficiency of the compressor
P_r_C_ch = P_r_C_ch; % [ ] charging compression ratio
% compression %
for i = 1:length(P_r_C_ch)

    [T_C_out_ch(i), P_C_out_ch(i), W_C_ch(i)] = compressor(T_C_in, P_C_in, P_r_C_ch(i), eff_C);

end

W_C_total_ch = W_C_ch .* (n_air_t_ch + n_air_TCES_ch) * on_sun * 60 * 60; % [J] total energy spent by the
compressor during charging

```

```

% power tower CSP %

for i = 1:length(P_r_C_ch)

    [T_t_in_ch(i), P_t_in_ch(i), Q_in_ch(i)] = powertower(T_C_out_ch(i), P_C_out_ch(i));

end

Q_CSP_total_ch = Q_in_ch .* (n_air_t_ch + n_air_TCES_ch) * on_sun * 60 * 60; % [J] total energy input from the
sun during charging

% main turbine %

eff_t = 0.8; % [ ] isentropic efficiency of the turbine

P_r_t_ch = (1.5)./(P_r_C_ch); % [ ] pressure ratio of the main turbine during charging

for i = 1:length(P_r_C_ch)

    [T_t_out_ch(i), P_t_out(i), W_t_ch(i)] = turbine(T_t_in_ch(i), P_t_in_ch(i), eff_t, P_r_t_ch(i));

end

W_t_total_ch = W_t_ch .* n_air_t_ch * on_sun * 60 * 60; % [J] total energy output from the turbine during
charging

% TCES %

for i = 1:length(P_r_C_ch)

    [T_TCES_out_ch(i), P_TCES_out_ch(i), n_air_TCES_ch(i)] = TCESCharge(n_react(i), T_t_in_ch(i), on_sun);

end

% TCES outlet and turbine outlet mixing to steam turbine %

eff_st = 0.8; % [ ] isentropic efficiency of the steam turbine

eff_sc = 0.8; % [ ] isentropic efficiency of the steam compressor

for i = 1:length(P_r_C_ch)

    T_mix(i) = air_mixing(T_t_out_ch(i), n_air_t_ch(i), T_TCES_out_ch(i), n_air_TCES_ch(i));

    [T_out_ch(i), P_out_ch(i), W_st_ch(i), W_sc_ch(i), Q_transf_ch(i), Q_s_cond_ch(i), mol_ratio_ch(i)] =
steam_turbine(T_mix(i), P_t_out(i), eff_st, eff_sc);

end

Q_trans_total_ch = Q_transf_ch .* (n_air_t_ch + n_air_TCES_ch) * on_sun * 60 * 60; % [J] total energy
transferred from the air to the steam cycle during charging

```

```

Q_s_cond_total_ch = Q_s_cond_ch .* (n_air_t_ch + n_air_TCES_ch) * on_sun * 60 * 60; % [J] total energy for
condensing the steam cycle during charging

W_st_total_ch = W_st_ch .* (n_air_t_ch + n_air_TCES_ch) * on_sun * 60 * 60; % [J] total energy output from the
steam turbine during charging

W_sc_total_ch = W_sc_ch .* (n_air_t_ch + n_air_TCES_ch) * on_sun * 60 * 60; % [J] total energy required for the
compressor in the steam cycle during charging

% net %

Q_in_ch = Q_CSP_total_ch; % [J] total thermal energy input from the sun

W_net_ch = W_C_total_ch + W_t_total_ch + W_st_total_ch + W_sc_total_ch; % [J] net work during charging

% % discharge % %

% compression %

T_C_in = 298; % [K] atmospheric temperature during discharge

P_C_in = 101325; % [Pa] atmospheric pressure during discharge

eff_C = 0.8; % [ ] isentropic efficiency of the compressor during discharge

P_r_C_dis = P_r_C_ch + 1; % [ ] pressure ratio of the compressor during discharge

% compression %

for i = 1:length(P_r_C_dis)

    [T_C_out_dis(i), P_C_out_dis(i), W_C_dis(i)] = compressor(T_C_in, P_C_in, P_r_C_dis(i), eff_C);

end

W_C_total_dis = W_C_dis .* n_air_dis * off_sun * 60 * 60; % [J] total compressor energy during discharge

% TCES discharge %

for i = 1:length(P_r_C_dis)

    [T_t_in_dis(i), P_t_in_dis(i), Q_TCES_dis(i)] = TCES_bed_dis(T_C_out_dis(i), P_C_out_dis(i));

end

% main turbine %

eff_t = 0.8; % [ ] isentropic efficiency of the turbine during discharge

P_r_t_dis = 1.5 ./ (P_t_in_dis/101325); % [ ] pressure ratio of the turbine during discharge

for i = 1:length(P_r_t_dis)

```

```

    [T_t_out_dis(i), P_t_out_dis(i), W_t_dis(i)] = turbine(T_t_in_dis(i), P_t_in_dis(i), eff_t, P_r_t_dis(i));

end

W_t_total_dis = W_t_dis .* n_air_dis * off_sun * 60 * 60; % [J] total energy from the main turbine during
discharge

% steam turbine %

eff_st = 0.8; % [ ] isentropic efficiency of the steam turbine during discharge

eff_sc = 0.8; % [ ] isentropic efficiency of the steam compressor during discharge

for i = 1:length(P_r_t_dis)

    [T_out(i), P_out(i), W_st_dis(i), W_sc_dis(i), Q_transf_dis(i), Q_s_cond_dis(i), mol_ratio_dis(i)] =
    steam_turbine(T_t_out_dis(i), P_t_out_dis(i), eff_st, eff_sc);

end

Q_trans_total_dis = Q_transf_dis .* (n_air_dis) * off_sun * 60 * 60; % [J] total energy transferred from the air
to the steam cycle during discharge

Q_s_cond_total_dis = Q_s_cond_dis .* (n_air_dis) * off_sun * 60 * 60; % [J] total energy required for condensing
for the steam cycle during discharge

W_st_total_dis = W_st_dis .* (n_air_dis) * off_sun * 60 * 60; % [J] total energy from the steam turbine during
discharge

W_sc_total_dis = W_sc_dis .* (n_air_dis) * off_sun * 60 * 60; % [J] total energy required for the steam
compressor during discharge

% net %

Q_in_dis = 0; % [J] thermal energy input from during discharge

W_net_dis = W_C_total_dis + W_t_total_dis + W_st_total_dis + W_sc_total_dis; % [J] net work during discharge

% % whole system net % %

Q_total = (Q_in_ch + Q_in_dis); % [J] total thermal energy input for one cycle

W_total = (W_net_ch + W_net_dis); % [J] total work for one cycle

% % analysis % %

whole_system_thermal_eff = - W_total ./ Q_total; % [ ] thermal to electric efficiency

P_max = interp1(T_t_in_ch, P_r_C_ch, T_max, 'spline'); % [Pa] max operating pressure limited by max CSP
temperature

eff_max = interp1(P_r_C_ch, whole_system_thermal_eff, P_max, 'spline'); % [ ] efficiency at max CSP temperature

m_stored = n_react * 153.33 / 1000; % [kg-Bao] mass of BaO that needs to be stored

```

```

V_stored = m_stored / (5.72 * 1000); % [m^3] volume of BaO that needs to be stored

V_max = interp1(P_r_C_ch, V_stored, P_max, 'spline'); % [m^3] volume of BaO required at max CSP temperature

split_ratio_max = interp1(P_r_C_ch, split_ratio, P_max, 'spline'); % [ ] air splitting ratio at max CSP
temperature

mol_ratio_ch_max = interp1(P_r_C_ch, mol_ratio_ch, P_max, 'spline'); % [ ] water to air molar ratio during
charging at max CSP temperature

mol_ratio_dis_max = interp1(P_r_C_ch, mol_ratio_dis, P_max, 'spline'); % [ ] water to air molar ratio during
discharge at max CSP temperature

n_air_ch = n_air_t_ch + n_air_TCES_ch; % [mol/s] total air flow during charging

n_air_ch_max = interp1(P_r_C_ch, n_air_ch, P_max, 'spline'); % [mol/s] total air flow during charging at max CSP
temperature

n_air_dis_max = interp1(P_r_C_ch, n_air_dis, P_max, 'spline'); % [mol/s] total air flow during discharge at max
CSP temperature

A_solar = Q_CSP_total_ch / on_sun / 60 / 60 / (Q_sun) * 10^(-6); % [km^2] solar array area

A_solar_max = interp1(P_r_C_ch, A_solar, P_max, 'spline'); % [km^2] solar array area at max CSP temperature

ch_eff = -(W_net_ch - W_C_ch .* n_air_TCES_ch * on_sun * 60 * 60) ./ (Q_CSP_total_ch - n_react .* 77.3 * 10^3);
% [ ] charging solar thermal to electric efficiency

ch_eff_max = interp1(P_r_C_ch, ch_eff, P_max, 'spline'); % [ ] charging solar thermal to electric efficiency at
max CSP temp

dis_eff = -W_net_dis ./ (n_react .* 77.3 * 10^3); % [ ] discharging solar thermal to electric efficiency

dis_eff_max = interp1(P_r_C_ch, dis_eff, P_max, 'spline'); % [ ] discharging solar thermal to electric
efficiency at max CSP temp

W_const = W_total / (on_sun + off_sun) / 60 / 60;

W_const_ch = W_net_ch / on_sun / 60 / 60;

W_const_dis = W_net_dis / off_sun / 60 / 60;

[max_eff, max_index] = max(whole_system_thermal_eff);

P_max_eff = P_r_C_ch(max_index);

%% plotting %%

% c_back = [173 173 173]/255;
% c_back = [235 235 235]/255;
c_back = [255 255 255]/255;

font_small = 20;
font_large = 28;

plot_line = 1;

```

```

line = 2.5;

% efficiency %

figure

set(gca, 'FontSize', font_small)

set(gca, 'fontname', 'times')

hold on

plot(P_r_C_ch, whole_system_thermal_eff * 100, 'k', 'LineWidth', line)
scatter(P_max, eff_max*100, 100, 'k', 'LineWidth', line)

xlabel('Charging Compression Ratio [ ]', 'FontSize', font_large)
ylabel('Solar to Electric Efficiency [%]', 'FontSize', font_large)

ylim([0 ceil(max(whole_system_thermal_eff)*100)])
xlim([min(P_r_C_ch) max(P_r_C_ch)])

pbaspect([1 1 1])

box on

set(gca, 'color', c_back)

set(gca, 'LineWidth', plot_line)

set(gcf, 'color', c_back)

% storage and area %

figure

set(gca, 'FontSize', font_small)

set(gca, 'fontname', 'times')

hold on

plot(P_r_C_ch, A_solar, '-k', 'LineWidth', line)
scatter(P_max, A_solar_max, 100, 'k', 'LineWidth', line)

xlabel('Charging Compression Ratio [ ]', 'FontSize', font_large)
ylabel('Solar Array Area [km^2]', 'FontSize', font_large)
ylim([0 ceil(max(A_solar))])

yyaxis right

plot(P_r_C_ch, V_stored, '-b', 'LineWidth', line)
scatter(P_max, V_max, 100, 'b', 'LineWidth', line)

ylabel('Volume of BaO Stored [m^3]', 'FontSize', font_large)

xlim([min(P_r_C_ch) max(P_r_C_ch)])
ylim([0 ceil(max(V_stored))])

```

```

set(gca,'ycolor','b')

box on

pbaspect([1 1 1])

set(gca, 'color', c_back)

set(gca, 'LineWidth', plot_line)

set(gcf, 'color', c_back)

hold off

% air and water flow ratios %

figure

set(gca,'FontSize',font_small)

set(gca,'fontname','times')

hold on

plot(P_r_C_ch, split_ratio, 'k', 'LineWidth', line)
scatter(P_max, split_ratio_max, 100, 'k', 'LineWidth', line)

xlabel('Charging Compression Ratio [ ]', 'FontSize',font_large)
ylabel('TCES Air Splitting Ratio [ ]', 'FontSize',font_large)

box on

pbaspect([1 1 1])

xlim([min(P_r_C_ch) max(P_r_C_ch)])

set(gca, 'color', c_back)

set(gca, 'LineWidth', plot_line)

set(gcf, 'color', c_back)

% air flow %

figure

subplot(1,2,1)

set(gca,'FontSize',font_small)

set(gca,'fontname','times')

hold on

plot(P_r_C_ch, n_air_ch * 3.6, 'k', 'LineWidth', line)

```

```

plot(P_r_C_ch, n_air_dis * 3.6, '--k', 'LineWidth', line)

scatter(P_max, n_air_ch_max * 3.6, 100, 'k', 'LineWidth', 2, 'HandleVisibility','off')

scatter(P_max, n_air_dis_max * 3.6, 100, 'k', 'LineWidth', 2, 'HandleVisibility','off')

xlabel('Charging Compression Ratio [ ]', 'FontSize',font_large)
ylabel('Total Air Flow Rate [kmol/hr]', 'FontSize',font_large)

ylim([0 ceil(max(n_air_ch)*3.6)])
xlim([min(P_r_C_ch) max(P_r_C_ch)])

legend('Charging', 'Discharging', 'Location','northwest')
legend boxoff
set(legend, 'color', c_back)

box on

set(gca, 'color', c_back)

set(gca, 'LineWidth', plot_line)

set(gcf, 'color', c_back)

pbaspect([1 1 1])

subplot(1,2,2)

hold on

set(gca, 'FontSize', font_small)

set(gca, 'fontname', 'times')

plot(P_r_C_ch, mol_ratio_ch, 'k', 'LineWidth', line)

plot(P_r_C_ch, mol_ratio_dis, '--k', 'LineWidth', line)

scatter(P_max, mol_ratio_ch_max, 100, 'k', 'LineWidth', 2, 'HandleVisibility','off')

scatter(P_max, mol_ratio_dis_max, 100, 'k', 'LineWidth', 2, 'HandleVisibility','off')

xlabel('Charging Compression Ratio [ ]', 'FontSize',font_large)
ylabel('Water to Air Molar Flow Ratio [ ]', 'FontSize',font_large)

xlim([min(P_r_C_ch) max(P_r_C_ch)])
ylim([0.2 0.5])

legend('Charging', 'Discharging', 'Location','northwest')
legend boxoff
set(legend, 'color', c_back)

box on

pbaspect([1 1 1])

set(gca, 'color', c_back)

```

```

set(gca, 'LineWidth', plot_line)

set(gcf, 'color', c_back)

hold off

% charging efficiency %
%
% figure
%
% hold on
%
% set(gca,'FontSize',font_small)
%
% set(gca,'fontname','times')
%
% plot(P_r_C_ch, ch_eff * 100, 'k', 'LineWidth', line)
%
% scatter(P_max, ch_eff_max * 100, 100, 'k', 'LineWidth', 2, 'HandleVisibility','off')
%
% xlabel('Charging Compression Ratio [ ]', 'FontSize',font_large)
% ylabel('Charging Solar to Electric Efficiency [%]', 'FontSize',font_large)
%
% xlim([min(P_r_C_ch) max(P_r_C_ch)])
%
% box on
%
% pbaspect([1 1 1])
%
% set(gca, 'color', c_back)
%
% set(gca, 'LineWidth', plot_line)
%
% set(gcf, 'color', c_back)
%
% hold off

% discharging efficiency %

figure

hold on

set(gca,'FontSize',font_small)

set(gca,'fontname','times')

plot(P_r_C_ch, dis_eff * 100, 'k', 'LineWidth', line)

scatter(P_max, dis_eff_max *100, 100, 'k', 'LineWidth', 2, 'HandleVisibility','off')

xlabel('Charging Compression Ratio [ ]', 'FontSize',font_large)
ylabel('Discharging TCES to Electric Efficiency [%]', 'FontSize',font_large)

xlim([min(P_r_C_ch) max(P_r_C_ch)])

```

```

box on

pbaspect([1 1 1])

set(gca, 'color', c_back)

set(gca, 'LineWidth', plot_line)

set(gcf, 'color', c_back)

hold off

% checking power %
%
% figure
%
% set(gca,'FontSize',font_small)
%
% set(gca,'fontname','times')
%
% hold on
%
% plot(P_r_C_ch, abs(W_const), 'k', 'LineWidth', line)
%
% plot(P_r_C_ch, abs(W_desired), '--k', 'LineWidth', line)
%
% plot(P_r_C_ch, abs(W_const_ch), 'r', 'LineWidth', line)
%
% plot(P_r_C_ch, abs(W_const_dis), 'b', 'LineWidth', 2)
%
% xlabel('Charging Compression Ratio [ ]', 'FontSize',font_large)
% ylabel('Work Output [W]', 'FontSize',font_large)
%
% xlim([min(P_r_C_ch) max(P_r_C_ch)])
% ylim([abs(W_desired(1))-10^7 abs(W_desired(1))+10^7])
%
% box on
%
% set(gca, 'color', c_back)
%
% set(gca, 'LineWidth', plot_line)
%
% set(gcf, 'color', c_back)
%
% pbaspect([1 1 1])
%
% hold off

```